POLITECNICO
MILANO 1863

SCUOLA DI INGEGNERIA INDUSTRIALE
E DELL'INFORMAZIONE

A FEM based study on wooden mechanical metamaterials

Tesi di Laurea Magistrale in
Music and Acoustic Engineering

Author: **Hakim El Achak**

Student ID: 978254
Advisor: Prof. Fabio Antonacci
Co-advisors: Dr. Sebastian Gonzalez
Academic Year: 2022-23

Abstract

The popularity of wood in stringed musical instruments is undeniable. Its workability, aesthetic, and its mechano-acoustic properties make it an ideal choice for their construction. Like many natural resources, wood is subject to variations even within samples taken from the same tree, making it a challenging task for instrument makers to maintain the exact same sound between one instrument and the next. Additionally, due to their unique properties certain species of wood have become endangered from excessive use.

This thesis aims to address these issues through the use of wooden mechanical metamaterials. Indeed, previous studies have demonstrated that the mechanical parameters of a wooden plate typically used for the construction of soundboards can be tuned via its perforation with periodic patterns of holes. Until now, only metamaterials with homogeneous hole dimensions have been studied for this purpose using the Caldersmith formulas to estimate their effective elastic constants. Our objective is to investigate how heterogeneous hole dimensions can affect the vibrational and mechanical behaviour of wooden plates. To this end, multiple configurations with heterogeneous hole sizes were investigated, and their impact on the elastic properties of the board measured via specifically designed solid equivalent plates. Said plates are used to find the material parameters which can make the vibrational behaviour of the equivalent plate and of the metamaterial match. In particular, a finite element model updating method was implemented to identify them by means of an optimization.

Our results show that the investigated wooden metamaterials have striking differences between homogeneous and heterogeneous hole size distributions. In fact, the stiffness of the plate is observed to be correlated to its hole size distribution, and a different behaviour can be found as well when studying them under dynamic or static conditions. This proves that a lot still has to be discovered about metamaterials but also that they are a powerful tool to be used in musical acoustics and beyond.

Keywords: Musical acoustics, mechanical metamaterials, finite element modeling, mechanical parameter identification, optimization

Abstract in lingua italiana

L'impiego del legno nella costruzione di strumenti musicali a corda è imperante. La sua lavorabilità, l'estetica e le sue proprietà meccano-acustiche ne fanno una scelta ideale. Come molte risorse naturali, il legno è soggetto a variazioni anche tra campioni prelevati dallo stesso albero, il che rende difficile mantenere costante la qualità del suono tra strumenti diversi dello stesso costruttore. Inoltre, per via delle loro proprietà uniche, l'impiego eccessivo di alcune specie arboree ha messo in pericolo la sopravvivenza delle stesse.

Questa tesi affronta questi problemi proponendo l'uso di metamateriali meccanici in legno. Infatti, studi precedenti hanno dimostrato che i parametri meccanici di una tavola lignea tipicamente utilizzata per la costruzione di tavole armoniche possono essere regolati attraverso la sua perforazione con pattern periodici di fori. Finora sono stati studiati a questo scopo solo metamateriali con fori di dimensioni omogenee, utilizzando le formule di Caldersmith per stimare le loro effettive costanti elastiche. Il nostro obiettivo è studiare come dimensioni eterogenee dei fori possano influenzare il comportamento vibrazionale e meccanico delle tavole lignee. A tal fine, sono state studiate diverse configurazioni con fori di dimensioni eterogenee e il loro impatto sulle proprietà elastiche della tavola è stato misurato studiando delle tavole equivalenti senza fori. Queste ultime sono state utilizzate per individuare i parametri del materiale che possano far coincidere il comportamento vibrazionale delle due tavole. In particolare, è stato implementato il metodo di ottimizzazione chiamato Finite Element Model Updating per l'identificazione di detti parametri.

I risultati mostrano che i metamateriali lignei studiati presentano notevoli differenze tra la distribuzione omogenee e quella eterogenea delle dimensioni dei fori. Infatti, si osserva che la rigidità della tavola è correlata a come i fori di diverse dimensioni sono distribuiti, e si riscontra un comportamento diverso anche nel loro studio in condizioni dinamiche o statiche. Questo prova che c'è ancora molto da scoprire sui metamateriali, ma anche che si tratta di un potente strumento da utilizzare nell'acustica musicale e non solo.

Parole chiave: Acustica musicale, metamateriali meccanici, modellazione a elementi finiti, identificazione dei parmetri meccanici, ottimizzazione

Contents

Introduction

Wood is the most used material in stringed musical instrument making. Its mechanical and acoustic properties, as well as its workability and appealing aesthetic, make it an ideal choice for the construction of musical instruments. Moreover, it is a natural resource that is available in abundance. Over the centuries, instrument makers have experimented with different types of wood and found the best species for each application. For example, softwoods such as Spruce are mostly used for soundboards, tropical woods like Pernambuco have become a standard for violin bows, and bamboo is extremely common in the bores of woodwinds [1]. However, some of these species are endangered making them unsustainable for the mass production of musical instruments [2]. In fact, they are often cut down illegally even though they are protected by CITES (Convention on International Trade in Endangered Species) [3]. Not to mention that global warming itself is changing the conditions of growth of wood causing variations in its properties [4].

In order to make more sustainable musical instruments, multiple studies have examined the material properties of these woods and explained why they excel at their role [5, 6]; Creating thus a correlation between classifications of woods made by the manufacturers of musical instruments, which are traditionally based on visual inspection of the samples of wood, and the physical material properties of these samples [7–9]. Knowing what material properties are desirable in order to achieve good acoustical quality is the key to finding alternative and more sustainable materials that can eventually replace the most used species of woods.

In particular, fiber-reinforced composite materials have received special attention as a suitable substitute for wood in musical instruments [10]. Composite materials are created by combining two or more materials with different physical and chemical properties, to obtain a new material with the desired characteristics. Generally, this is done by embedding strong fibers within a light polymer matrix. Recent studies have measured the acoustic qualities of composite materials and compared them to those of traditional woods [11]. Patents of bowed string instruments made of composite material have also already been published [12]. In [11], the authors demonstrated that composite materials can have exceptional acoustic properties. Especially in the case of carbon fiber reinforced

composites, which, although characterized by a much higher density, can also achieve a very large specific longitudinal Young's modulus and lower damping ratio than those of traditional woods. Both of which are good indicators of acoustic quality. Furthermore, a water absorption test revealed that composite materials are also more resistant than wood to environmental conditions such as humidity, making them more stable and reliable. Despite these advantages, wood is still the preferred material by most luthiers and musicians. Perhaps because the longer history makes it difficult for it to be replaced by a completely different material.

Even though composite materials are a promising alternative to wood, another common approach is that of using other, more sustainable wood species by enhancing their properties to match those of the ideal woods through physical or chemical alteration. Some examples are thermally modified woods [3], and chemically altered woods [13, 14] that have been demonstrated to be adequate substitutes for specific acoustic situations. This approach makes it possible to keep using wood as the primary material, but in a more sustainable manner.

Finally, we have metamaterials which have been the focus of more and more research, especially in the last decades, because of their unusual and malleable properties. This thesis focuses on their use with the objective of manipulating the mechanical properties of any piece of wood in order to make it usable in instrument making. Metamaterials are born from the advancement of technologies making it possible to build materials at smaller scales. In fact, by altering the micro-structure of these materials, sometimes even at nanometric scales, it is possible to obtain mechanical and acoustic properties that cannot be found in conventional materials [15, 16]. Some examples of exotic material parameters are negative poisson ratios in auxetic metamaterials such as the one represented in Figure 1 and negative refraction coefficients. The latter is particularly appreciated in acoustic applications where metamaterials are used for acoustic imaging and acoustic lenses among other applications [17, 18].

One of the most recent and innovative ways of taking advantage of the properties of metamaterials is to use them in the instrument making process. Not only to manipulate the spectrum of sounds of the instrument [19, 20], but also to tune the elastic properties of wood. In fact, it has been demonstrated by the authors in [21] that the use of periodic hole patterns on rectangular wooden boards allows the mechanical and acoustic properties of the board to be controlled. This result could potentially give the possibility to instrument makers to start from any piece of wood and fine tune its material properties to reach or even surpass those of the traditionally used wood species. Creating a sustainable alternative to endangered woods, and opening up entirely new possibilities both

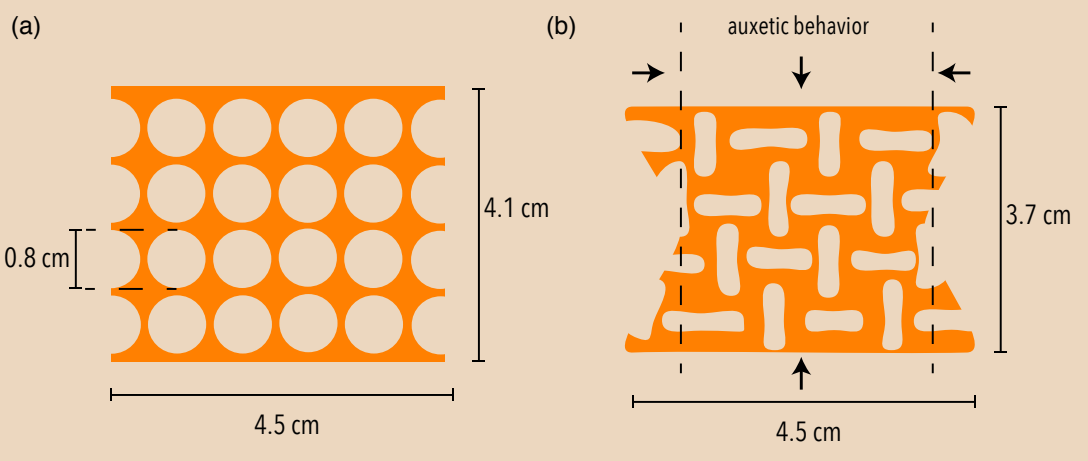

Figure 1: (a) Mechanical metamaterial in a relaxed state: squared arrays of circular holes in an elastomer matrix. (b) Metamaterial with a deformation of 11 % : during the compression, the square array of circular holes is transformed upon reaching a critical deformation, into a periodic pattern of alternating, mutually orthogonal, ellipses [19].

acoustically, and aesthetically in the making of the instrument. This result has also been confirmed experimentally showing that there is a bijective relation between the density of the board and it's longitudinal stiffness [22], and applied numerically to the model of a classical guitar proving that metamaterials can be integrated in an instrument to tune its response without compromising its structural integrity [23].

Since an accurate non destructive experimental measure of the elastic properties of the perforated wooden boards is difficult to implement, most of the mentioned studies rely on Caldermith's formulas to calculate the stiffness of the wooden samples [24]. These formulas allow the user to approximate the value of the elastic properties of rectangular wooden plates based on their dimension, density, and vibrational properties. The aim of this thesis is to verify the accuracy of this approximation in the case of metamaterials, find a way of improving it through the use of numerical simulations and optimization algorithms, and use the results to investigate the effect of the metamaterials on the mechanical and vibrational properties of wood. This is done by creating 3D models of a set of rectangular metamaterial wooden plates characterized by various patterns of holes that will be used as reference, and then attempt to find the material properties of an equivalent plate with the same vibrational properties, i.e. the same eigenfrequencies and modeshapes. These equivalent plates are defined by being solid plates, meaning no holes are drilled in them, and by having the same length, width and height as their corresponding reference plates.

The process of finding the material parameters of the equivalent plate that better fit the eigenfrequencies and modeshapes of the reference plate is done through an optimization

algorithm utilizing the finite element model updating method that will be explained in detail in Chapter 2. The obtained equivalent plates can give us insight about the influence of different metamaterial configurations on the material parameters of wood. These plates are then tested as well in static conditions, conducting numerical experiments with a static load and varying boundary conditions in order to verify their mechanical behavior. Finally, the influence of metamaterials on the Poisson ratio of the plates is investigated considering also the possibility of having a negative coefficient.

The relevance of identifying accurate equivalent plates with simple geometries goes beyond the fact of being able to verify the Caldersmith formulas. In fact, one could use these results with the objective of training an artificial intelligence capable determining the right pattern of holes to apply to a certain wooden board with known material properties in order to tune in and obtain other, more desirable properties. The advantage of using the equivalent plates for such an application is that the meshing process of a regular rectangular plate without any holes is much easier and less computationally expensive than that of a plate with multiple circular or even more complex geometries.

Thesis outline

The thesis is organized in the following manner:

First, after an introduction contextualizing and explaining the aim of this work, **Chapter 1** goes through the relevant background concepts utilized in this thesis. Starting with a description of wood's linear elastic and orthotropic material properties, we then dive into modal analysis techniques used in characterization of the vibrational properties of any object, explaining as well how the previously mentioned Caldersmith formulas can be used as a non destructive technique of material parameter approximation for wooden rectangular thin boards. Finally, This chapter ends with a description of the basics of the finite elements methods which is extensively used throughout the whole thesis.

Then, in **Chapter 2**, the methods utilized for studying the equivalent plates and the identification of their material parameters are analyzed. More specifically, a detailed description of the built 3D geometries for the reference plates is given considering both homogeneous and heterogeneous distributions of hole dimensions in the metamaterial. After that, the various equivalent models studied are described with all their particularities, and in the end, the process of material parameter identification using the finite element model updating optimization method is exhaustively explained.

Chapter 3 contains all the results of the thesis. First, the homogeneous metamaterial configuration is studied, using the Caldersmith formulas to find the material parameters of the equivalent plate and comparing the accuracy of those results to the ones obtained using the optimization method. Subsequently, heterogeneous configurations of hole dimensions are investigated. In particular, different equivalent plate models are tested and confronted to each other and to the Caldersmith method with and without optimization of the material parameters. Once a good enough equivalent plate model is found, its behaviour in response to a static force is studied, and the possibility of having a negative Poisson ratio is verified through a tensile test. Finally, the material parameters of the equivalent plates of heterogeneous metamaterial configurations are analyzed and their possible applications discussed.

At last, in **Chapter 4**, conclusions are drawn looking back at what was achieved during this thesis, and possible ideas for future developments are explored.

1 | Background

The aim of chapter is to give a description of all the fundamental concepts required in the context of this thesis. Starting with an explanation of the mechanics of linear elastic materials and their properties, we will then see how the orthotropic nature of wood influences these properties and how modal analysis makes it possible to study the vibrational properties of a system. From here, we will describe the Caldersmith formulas and how they can be used to retrieve the main elastic properties of a rectangular wooden plate in a non destructive way and see that with the help of the finite elements method, all these concepts can be applied in the context of numerical simulations.

1.1. Mechanics of solids

1.1.1. Linear elastic materials

In mechanics, problems are treated differently depending on the material behaviour [25]. The material determines the model, equations and material properties that need to be used to solve the problem under hand. Wood in particular is considered a linear elastic orthotropic material [26]. These keywords are very important as they define the mechanical behaviour of wood. A linear elastic material is characterized by a deformation that depends linearly on the load that is applied onto it, in addition to the elasticity property which implies that after the load is removed, the object will recover its original shape with no residual deformation. This property is valid for low stress and deformations while at higher stress levels plastic deformation or failure will occur.

In the linear elastic region, the relationship between stress and deformation is governed by the general formulation of Hooke's Law. For a generic anisotropic material, which is a material whose properties vary depending on the considered direction, the stress–strain relationship is a tensorial equation:

$$\sigma_{ij} = C_{ijkl}\varepsilon_{kl}$$

Where σ_{ij} is the stress tensor, ε_{kl} is the infinitesimal strain tensor and C_{ijkl} is the elastic modulus (or stiffness) tensor.

This relation can be inverted using the elastic compliance tensor S_{ijkl} instead of C_{ijkl}.

$$\varepsilon_{ij} = S_{ijkl}\sigma_{kl}$$

C_{ijkl} and S_{ijkl} are fourth-order tensors meaning they each should have 81 components. Fortunately, since the stress and strain tensors are symmetric, the following symmetries apply to linear elastic materials and the number of components is thus reduced to 21:

$$C_{ijkl} = C_{klij} = C_{jikl} = C_{ijlk}$$

Additionally, if a material has a symmetry plane, then applying stress normal or parallel to this plane introduces deformation only in directions normal and parallel to the plane. Orthotropic materials such as wood have three mutually perpendicular symmetry planes. This reduces the number of independent material parameters to 9 and the general stress-strain relation of an orthotropic material is expressed as:

$$\begin{bmatrix} \varepsilon_{11} \\ \varepsilon_{22} \\ \varepsilon_{33} \\ \varepsilon_{23} \\ \varepsilon_{13} \\ \varepsilon_{12} \end{bmatrix} = \begin{bmatrix} 1/E_1 & -\nu_{21}/E_2 & -\nu_{31}/E_3 & 0 & 0 & 0 \\ -\nu_{12}/E_1 & 1/E_2 & -\nu_{32}/E_3 & 0 & 0 & 0 \\ -\nu_{13}/E_1 & -\nu_{23}/E_2 & 1/E_3 & 0 & 0 & 0 \\ 0 & 0 & 0 & 1/2G_{23} & 0 & 0 \\ 0 & 0 & 0 & 0 & 1/2G_{13} & 0 \\ 0 & 0 & 0 & 0 & 0 & 1/2G_{12} \end{bmatrix} \begin{bmatrix} \sigma_{11} \\ \sigma_{22} \\ \sigma_{33} \\ \sigma_{23} \\ \sigma_{13} \\ \sigma_{12} \end{bmatrix}$$

The compliance tensor contains all nine of the independent material parameters needed to express the relation between stress and strain. Even though the compliance tensor contains six different Poisson's ratios, they are connected by the following symmetry property:

$$\frac{\nu_{ij}}{E_i} = \frac{\nu_{ji}}{E_j} \qquad \text{for } i \neq j$$

Meaning only three of them are necessary to properly identify the orthotropic material.

Below is a definition and explanations of each parameter:

The **Young modulus** E_i, as expressed by Hooke's law:

$$\sigma_{ii} = E_i \varepsilon_{ii}$$

is the slope of the stress-strain curve in uni-axial tension. An orthotropic material can have three different values of E_i. One for each principal direction. The Young's modulus gives an idea of the stiffness of the material in a specific direction.

The **shear modulus** G_{ij} on the other hand is the ratio of the shear stress τ to the shear strain γ and is defined as :

$$G_{ij} = \frac{\tau_{ij}}{\gamma_{ij}}$$

Known also as the modulus of rigidity, it indicates the response of the material to shear stress. Just like Young's modulus, it also needs three different values to properly define a material.

Poisson's ratio ν_{ij} is a measure of the compressibility of a solid. The Poisson effect happens when a load applied in a specific direction causes a deformation in perpendicular directions. This phenomenon is commonly observable when pressing down on a piece of rubber and noticing that the sides expand as a result. It is defined as the negative ratio of the transverse strain to the axial strain:

$$\nu_{ij} = -\frac{\varepsilon_j}{\varepsilon_i}$$

Typical values range from 0.2 to 0.49 with some notable cases being $\nu = 0.5$ meaning that the material is incompressible and $\nu = 0$ where stretching the solid doesn't cause any lateral deformation. Some metamaterials can even have negative Poisson ratio meaning that stretching the specimen in a specific direction causes a lateral expansion. Also in this case, three different Poisson's ratios define an orthotropic material.

1.1.2. Wood as an orthotropic material

As mentioned earlier wood is considered an orthotropic material. Its orthotropic nature is due to the grain growing in a specific direction and to the formation of growth rings. Because of this, one can define a set of three mutually perpendicular directions, each with

different mechanical properties.

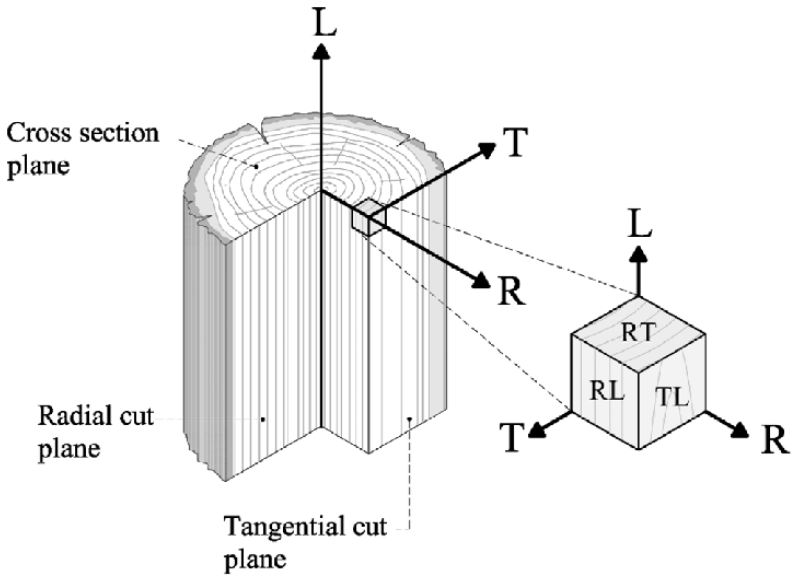

Figure 1.1: Main orthotropic directions and planes in wood [27].

The axis parallel to the direction of the grain is called the longitudinal direction **L**. Generally, this is the direction with highest stiffness due to the fibers being all parallel to this axis. The axis perpendicular to the longitudinal one and normal to the growth rings is the radial direction **R**. The last axis is still perpendicular to the longitudinal one but tangent to the growth rings. It is called the tangential axis **T**. Figure 1.1 is taken from [27] and does an excellent job illustrating the main axis of a wooden piece.

From this point onward we will use the subscripts **L**, **R**, and **T** to refer to the Longitudinal, Radial and Tangential directions respectively.

1.2. Modal analysis

When it comes to studying the dynamical characteristics of a structure, modal analysis is a very powerful tool. With it, it is possible to determine the natural frequencies, damping factors and mode shapes of a system, and use them to formulate a mathematical model for its dynamic behaviour [28]. This is particularly interesting when designing soundboards for musical instruments as they are the main protagonist in terms of sound radiation. For that reason, particular attention is given to tuning the soundboard in order to emphasize specific frequencies and make the resulting sound more pleasing.

Musical instrument makers are known to consistently use modal analysis not only for tuning the soundboard but also in the process of selecting a good wood sample. They

do it by using the **tap tones method** [29], which consists in holding the plate of wood between forefinger and thumb at a node location for the inspected mode, and tap with a knuckle or other finger at the location of an anti-node. This method require a lot of expertise and knowledge about the mode shapes to be able to estimate the position of nodes and anti-nodes of a particular mode shape, as well as a tuner or a well trained ear to identify the frequency of that particular mode.

Another more popular and precise way to perform modal analysis is by using **Chladni patterns** [30]. This method involves scattering small particles such as sand or salt on a thin plate, and by exciting said plate at specific frequencies called eigenfrequencies, the plate will start to vibrate in a determined way forming what we call a mode shape. The excitation of the plate can happen in various ways, one of the most used ones is by placing a sound source under it and play a pure tone sweeping the inspected frequency range, and stopping when the particles start reacting strongly to the vibration as this is an indicator that a resonance point has been reached. The particles will then accumulate on the nodal lines of vibration which are regions of the plate that don't vibrate at that particular frequency. An example of this process can be observed in Figure 1.2 where Chaldni patterns are used to verify the frequency mode shapes of an assembled guitar top plate [31].

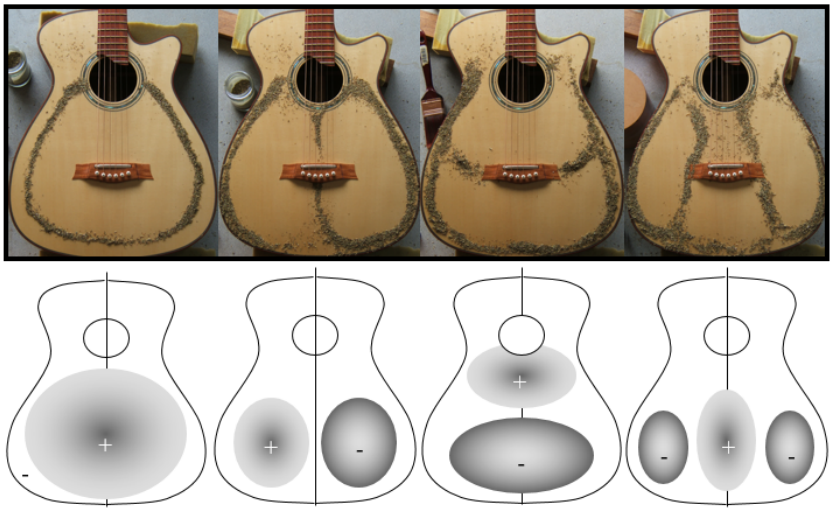

$T(1,1)_x$	T(2,1)	T(1,2)	T(3,1)
Main Top Monopole	Cross Dipole	Long Dipole	Cross Tripole
100, 181, 217Hz	304Hz	404Hz	448Hz
A B C	D	E	F

Figure 1.2: Modal analysis of a guitar top plate using Chladni patterns [31].

The most accurate way of performing modal analysis is by calculating or measuring the **Frequency Response Function** (FRF) of the system. This function, also called transfer function, is defined as the ratio of the output to the input of a linear time invariant system where the input is a known excitation force, and the output can be either the displacement, velocity or acceleration in another point. The FRF can be obtained in multiple ways:

- **Analytically**, with knowledge of the equation of motion of the system as well as its mass, stiffness and damping parameters.
- **Experimentally**, by measuring the response of the system in one point after exciting it with a known input applied on another point. From this information we can extract the transfer function of the system although it can be a very time consuming process to acquire this data for a large quantity of points on the measured object.
- **Numerically**, by applying the Finite Element Method (FEM) that will be discussed in Section 1.4.

This last method will be the preferred one as it allows fast and precise computation the eigenfrequencies and mode shapes of a system which will be crucial in analyzing the behavior of a set of reference metamaterial plates and finding the material parameters of the equivalent solid plates that match the same eigenfrequencies and mode shapes as we will see in Chapter 2.

1.3. Material parameter identification and Caldersmith formulas

The identification of material parameters often requires tensile tests of a sample of the material to be investigated. By applying a slowly varying known stress in a specific direction, and measuring the strain in the others, one can easily measure the elastic properties of a material using the relations described in Section 1.1.1. The main problem with this method is that it needs to be repeated for each principal direction for an orthotropic material and more importantly, it involves the destruction of the used samples. For a natural material such as wood, the properties can vary easily between samples because of imperfections of the grain and growth rings. Because of this, although slightly less accurate, non-destructive methods are often used to determine the material properties of samples.

In the particular case of thin rectangular wooden plates, various studies in the literature have shown that it is possible to get a good approximation of the main elastic properties

from their vibrational qualities [24, 32]. More precisely, for a thin rectangular wooden plate with sides of length a and b, thickness h and density ρ, we can estimate the value of the longitudinal and radial Young's moduli E_L and E_R, as well as the longitudinal to radial Shear modulus G_{LR} as:

$$\begin{cases} E_L &= 12 \times \dfrac{0.08006\, \rho\, a^4\, f_{(0,2)}^2}{h^2} \\ E_R &= 12 \times \dfrac{0.08006\, \rho\, b^4\, f_{(2,0)}^2}{h^2} \\ G_{LR} &= 3 \times \dfrac{0.4053\, \rho\, a^2\, b^2\, f_{(1,1)}^2}{h^2} \end{cases} \tag{1.1}$$

Where $f_{(0,2)}$ is the frequency of the fundamental long grain bar mode, $f_{(2,0)}$ is the frequency of the fundamental cross grain mode and $f_{(1,1)}$ i the frequency of the twisting mode. The mode shapes of these modes can be observed and easily recognized from the Chladni patterns in Figure 1.3.

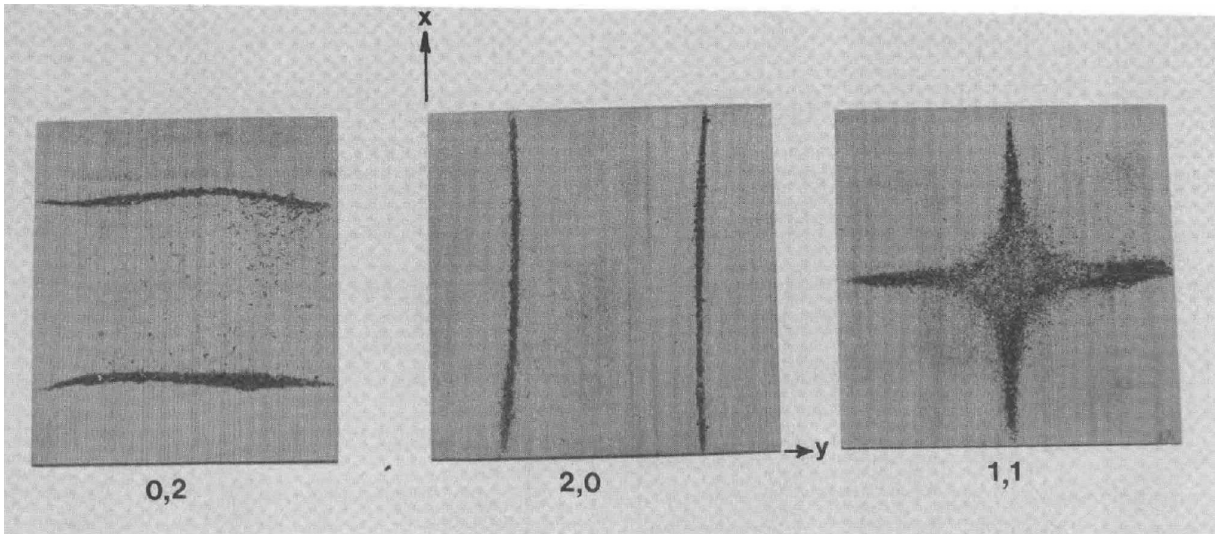

Figure 1.3: Chaldni patterns of the vibrating modes needed to use Caldersmith's formulas [24].

It is worth pointing out that the coefficients in equations 1.1 are not always the same in the literature. In fact, the ones reported in the equations are the ones derived by Caldersmith but a different coefficient for G_{LR} can be found in the paper by McIntyre and Woodhouse [32] where they use a coefficient of 0.274 instead of 0.4053. The difference is probably due to an approximation made for the twisting deformation employed to estimate G_{LR}.

During our study, we will use the Caldersmith formulas with both coefficients to get an approximation of the material parameters of our equivalent plates using as data the infor-

mation we have about the reference metamaterial plates. By using numerical simulation tools such as the FEM described in the next section, we will be able to compare the mode shapes and eigenfrequencies of the reference plates and the equivalent plates obtained with the Caldersmith formulas.

1.4. Finite Element Method

Many problems in physics are governed by partial differential equations that cannot be solved analytically. Because of this, over time, various methods have been proposed to simplify complex problems and approximate the solution through discretization. Some examples include finite difference methods and variational methods [33]. To the best of our knowledge, the most used numerical method to solve complex engineering problems is currently the Finite Element Method (FEM) as it has been successfully applied to multiples fields such as heat conduction, fluid dynamics, electric and magnetic fields [34], and noticeably also in acoustics [35–37].

The basic idea of FEM is to discretize a continuous object into a sum of sub-spaces called elements. These elements are often characterized by a simple geometry to reduce the complexity of the problem and are always interconnected at specified joints called nodes. At the end of this discretization process we obtain a mesh of the studied object which is the sum of the elements and nodes defined before. We then use this mesh to compute the solution of the problem at the nodes and use shape functions to get an approximated solution inside each element.

As an example, let us examine the case of a 1D problem illustrated by [38]. We consider a function u that could represent the wave equation in a string which is represented by a partial differential equation. u can approximated with a function $u_h \approx u$ using linear combinations of basis functions according to the following expression:

$$u_h = \sum_i u_i \varphi_i$$

Where φ_i are the basis functions and u_i are the coefficients of the functions that approximate u with u_h. Figure 1.4 illustrates this principle. Here, the linear basis functions have a value of 1 at their respective nodes and 0 at other nodes. In this case, there are seven elements along the portion of the x-axis, where the function u is defined (i.e., the length of the string).

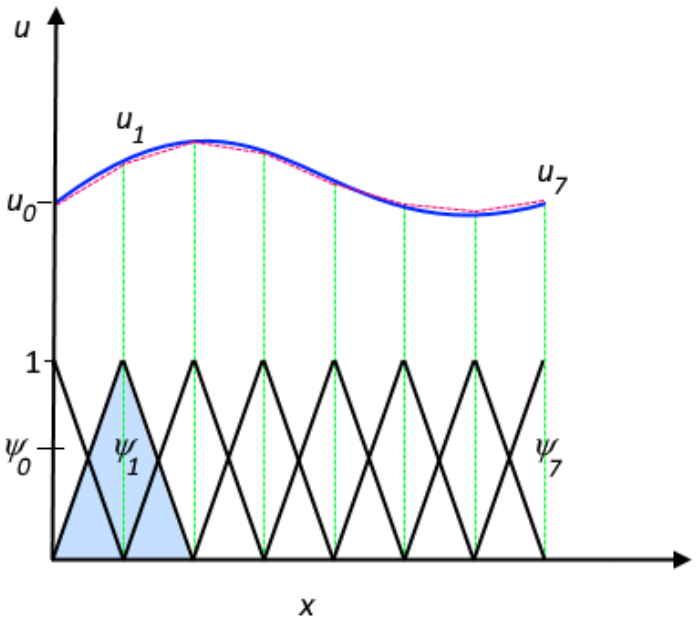

Figure 1.4: The function u (solid blue line) is approximated with u_h (dashed red line), which is a linear combination of linear basis functions (φ_i is represented by the solid black lines). The coefficients are denoted by u_0 through u_7 [38].

To summarize, the FEM process can be described in the following steps [39]:

- Establishing the governing equations of the problem and the boundary conditions
- Discretizing the domain
- Determining the algebraic element equations
- Assembling system global equations
- Imposing the boundary conditions of the problem
- Solving of the global equations

This is obviously an abridged explanation of how FEM works as explaining it in detail would require a whole book [33]. More often than not, FEM is used through commercial simulation softwares such as COMSOL that allow their user to use FEM models to solve various physics related problems. In our study, we use that exact software to solve the equations of motion of the studied wooden plates and extract from them information about the mode shapes and eigenfrequencies.

2 | Methods

This chapter focuses on the methodological aspects involved in the work of this thesis. The aim is to analyze multiple configurations of metamaterial patterns studying their influence on the material parameters of a wooden plate. To achieve this, 3D geometries of thin rectangular wooden boards with specific hole patterns are created to be used as reference. In order to find out how various hole patterns affect the material parameters of the board, an equivalent plate with the same length, width and height as the reference, but no holes drilled in it, is considered. Finding the material parameters that make the equivalent plate's vibrational behavior comparable to that of the reference makes it possible to get a good approximation of its effective material parameters.

The chapter is divided into different sections; Firstly, a detailed description of the different reference and equivalent model geometries is given. Then, the two methods used for the identification of their material parameters are discussed. The Caldersmith's formulas method is explained first, before analyzing the second one which relies on an optimization of the material parameters through the minimization of an error function. More specifically, the defined objective function and the metrics used to evaluate it are discussed, paying attention also to the chosen optimization algorithm as well as the initial conditions and boundaries of each parameter.

2.1. Reference plates

The definition of metamaterials as explained in the introduction is broad. In fact, creating one from a wooden plate can be done in an infinite amount of ways. This thesis in particular is based on the study done in [21], where the authors used patterns of elliptical holes with various sizes, aspect ratios and orientations to observe their effect on the material properties of a wooden plate. Our first objective is to take as reference a plate with the same hole patterns as in the above mentioned article, recreating a model with the same geometry, material parameters, physics and boundary conditions on COMSOL. The plates in [21] are characterized by having holes all of the same dimensions. The aim here is to go beyond these results and study configurations with heterogeneous hole

dimensions in order to see how they behave compared to the homogeneous case.

2.1.1. Homogeneous configurations

The models used in this thesis are created using COMSOL's built-in model builder which allows the user to design 3D geometries of simulated objects, assign them the desired material properties, and define the physics of the problem. Furthermore, the possibility to run the FEM modal analysis simulations on COMSOL with no need to switch platforms makes it the ideal choice of software for this study.

The wooden plates studied in [21] are thin rectangular boards cut along the tangential direction. The main surface of the board is in the **RL** plane shown in Figure 1.1, with the grain direction **L** being parallel to the longest side of the rectangle. The dimensions of the board are those of a common cut used for guitar soundboard top plates: $0.6 \times 0.24 \times 0.0035$ $[m]$. The method used in the article to make a metamaterial from that wooden board is to perforate it at regular intervals with elliptical holes all of the same dimension. This is achieved by dividing the plate in a set of identical square cells as can be seen in Figure 2.1.

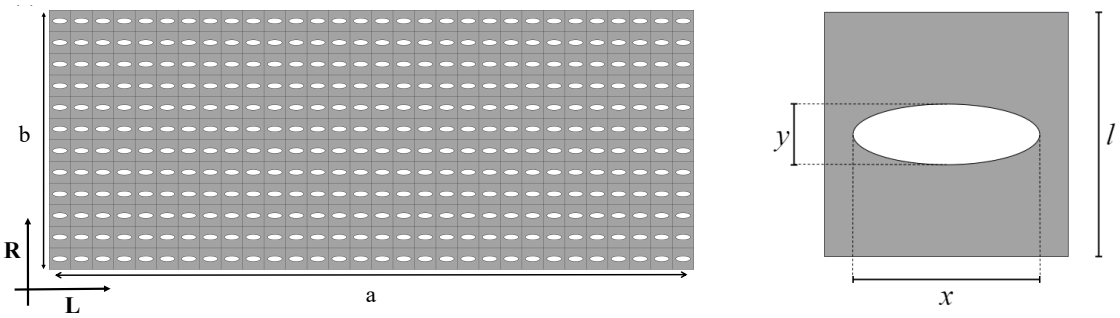

(a) Top view of the rectangular plate.

(b) The unitary cell repeated in the plate.

Figure 2.1: Geometry of the studied plate.

The cell's sides length is $L = 0.02$ $[m]$ and the elliptical hole drilled in it has its major axis orientated in the longitudinal direction of the plate **L**. The aspect ratio of the ellipse is $x/y = 2.2$, and the volume fraction of the hole with respect to the cell is $V_h = 0.15$. These details have been carefully defined in the numerical model in order to recreate the same plate studied in the aforementioned paper. This makes it possible to verify the validity of the vibrational results obtained from the reference plate as well as using them as ground truth for comparison with the equivalent plates.

2.1.2. Heterogeneous configurations

While the effects of homogeneous hole size distributions on a wooden board have already been studied in [21], the behaviour caused by the presence of various distributions of holes sizes on the board has not yet been investigated. This could be an interesting tool for example for guitar makers who wish to make some parts of their soundboards lighter than others, or in the violin making process where the graduation of the plates is of high relevance. In order to study how heterogeneous hole size distributions in the metamaterial can affect the properties of the plate, let us consider a set of 22 plates, each with a different configuration of hole dimensions but all having the same constant density. Figure 2.2 shows 10 of these configurations.

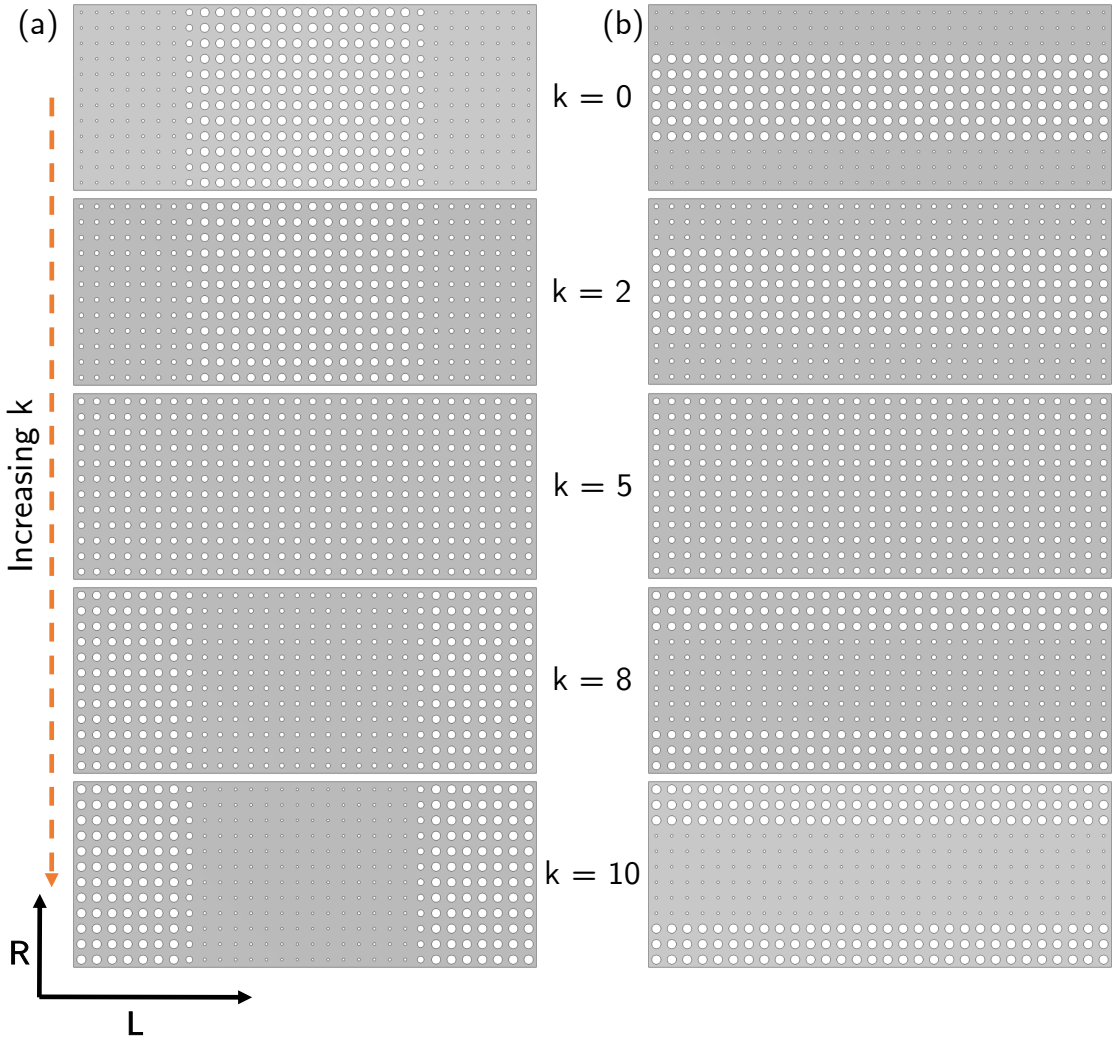

Figure 2.2: Heterogeneous reference plate configurations for radial symmetry (a) and longitudinal symmetry (b).

The set is divided into 2 groups with the objective to cover various distributions of hole sizes along the plate. One group is made of plates whose hole dimensions are symmetric with respect to the longitudinal direction, and the other contains plates whose hole dimensions have radial symmetry. In the group with longitudinal symmetry, the holes start with a smaller radius near the edges of the plate parallel to the longitudinal directions and grow bigger as they get close to the horizontal axis of symmetry. The same is true considering the radial direction and the vertical axis of symmetry for the plates with radial symmetry. Considering an index k going from 0 to 10, the different configurations in the same group consist in gradually inverting the hole dimensions while keeping the total density of the plate constant until the holes with largest radius in configuration $k = 0$ become the smallest ones in configuration $k = 10$, and the opposite process happens to the smallest holes. For configuration $k = 5$, all the holes are of same dimension making it a special case of homogeneous configuration within the set. Considering the higher number of configurations examined in this section, studying the effect of various shapes for the holes would drastically increase the number of cases of study. Due to this, only holes of circular shape will be considered for all configurations.

2.2. Equivalent plates

The role of the equivalent plates is to measure the elastic constants of the studied metamaterials. While in the study of homogeneous metamaterials conducted in [21] their elastic constants were approximated using the Caldersmith formulas, the objective here is to try to understand the behaviour of the metamaterials through the study of equivalent solid plates since they are what is commonly used and well understood by instrument makers. The effective material parameters of the equivalent plates are found by searching for the parameters that make the equivalent plate's eigenfrequencies and mode shapes as similar as possible to that of its corresponding reference plate. These parameters can then be analyzed to understand the effect various hole patterns can have on a wooden board. This section goes through multiple models of equivalent plates created with the aim of improving the accuracy with which the vibrational behaviour of the reference plates is reproduced.

2.2.1. Homogeneous model

The first equivalent model considered is also the simplest one. It consists in a solid representation of the reference plate. In fact, as can be seen in Figure 2.3, it is a solid rectangular thin plate with the same dimensions as the reference. Although its material

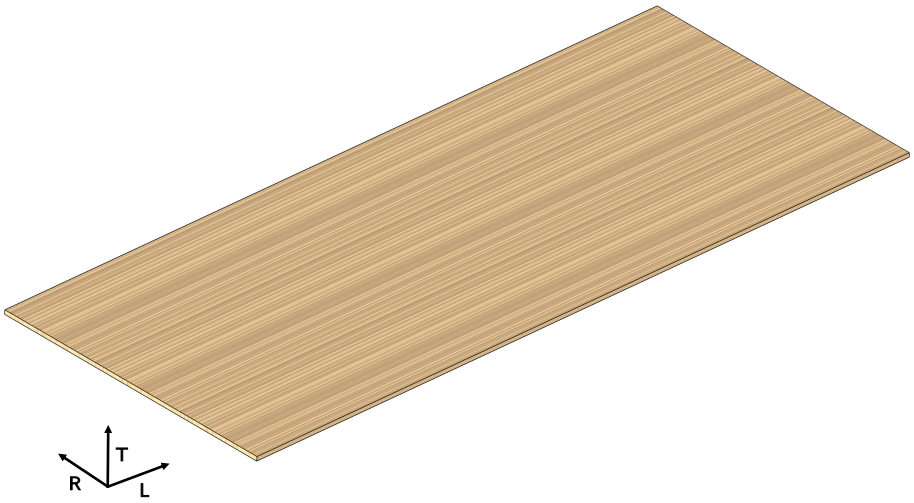

Figure 2.3: 3D representation of the homogeneous equivalent plate model. Its dimensions are the same as the reference plate i.e. $0.6 \times 0.24 \times 0.0035$ $[m]$.

parameters will be different to take into account the effect of the metamaterial, its structure is still defined as orthotropic with the longitudinal direction being parallel to the longest side of the plate. As will be demonstrated in the Results chapter, this equivalent plate may work well in the case of homogeneous configurations of hole sizes, but its constant density makes it difficult to capture the uneven mass distribution caused but the heterogeneous hole sizes configurations.

2.2.2. Variable thickness model

In order to take into account the different mass distribution on the reference plates with heterogeneous configurations, let us consider as well a model of the equivalent plate where the thickness of the plate is calculated to reflect the equivalent mass of the reference plate at that point. As previously seen in Figure 2.1, the metamaterial is divided in cells. And in the case of our heterogeneous configurations, it can be seen in Figure 2.2 that the cells are all identical in the direction of the considered axis of symmetry. Because of this, it is possible to define a constant thickness profile for each given configuration to match the effective mass of each cell as in Figure 2.4.

The equivalent thickness is calculated on the red dots which correspond to the center of the unitary cells delimited in Figure 2.4 by thin dotted lines. The only exception being the first dot which is needed to define the thickness at the boundary. The thickness is calculated so that the mass of the equivalent plate's solid cell matches that of the reference plate's considered cell. Mathematically, the mass of the equivalent plate's cell is

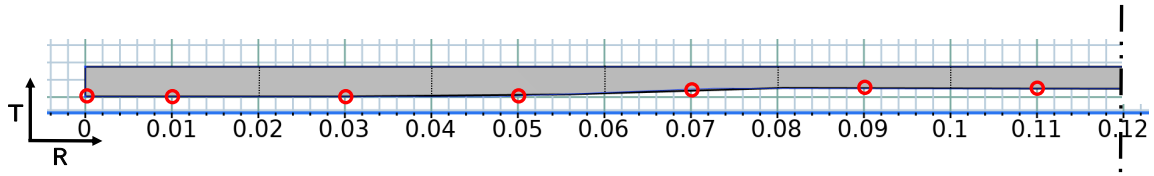

Figure 2.4: Profile section in the **TR** plane of the variable thickness equivalent plate of longitudinal configuration $k = 0$. The red dots correspond to the calculated points used to interpolate the thickness of the equivalent plate. At 0.12 m is the axis of symmetry of the plate.

approximated as the density of the plate multiplied by the volume of the equivalent cell. The curvature of the profile can be neglected in this calculation by taking the value of the thickness at the center of the cell. This translates into the following relation:

$$\rho \times h_{eq} \times l^2 = \rho \times h_{ref} \times (l^2 - \pi R^2) \tag{2.1}$$

$$h_{eq} = h_{ref} \left(1 - \frac{\pi R^2}{l^2}\right) \tag{2.2}$$

Where ρ is the density of the plate, h_{eq} and h_{ref} are the thickness of the equivalent and reference cells respectively, l is the length of the side of the cells, and R is the radius of the hole in the considered cell of the reference plate. The thickness profile is then drawn using an interpolation curve connecting all the calculated points.

2.2.3. Variable density model

Another way to tackle the problem of varying mass in the reference plate is that of using a variable density in the equivalent plate rather than a variable thickness. This method has the advantage of preserving the original dimensions of the reference plate varying only the material parameters of the equivalent plate. Two different density models are considered in this section. In the first one, the equivalent density of each file (i) of cells is calculated according to the volume fraction of its hole size. That density is the attributed to the whole file using a similar formula to the one used for the variable thickness equivalent plates:

$$\rho_{eq}(i) = \rho_{ref} \left(1 - \frac{\pi R(i)^2}{l^2}\right) \tag{2.3}$$

The result is a piece-wise constant variation of the density along the profile of the plate

as can be observed in Figure 2.5.

In the second one, the density is made to vary linearly inside the plate with a slope and intercept that can be modified and optimized to better match the mass distribution of the reference plate. The equivalent density is approximated by a simple linear function:

$$\rho_{eq}(x) = dx + \rho_0 \tag{2.4}$$

Where d is the slope, ρ_0 the intercept, and x is the position along the radial direction if we consider a longitudinal symmetry reference plate, or the position along the longitudinal direction in the opposite case.

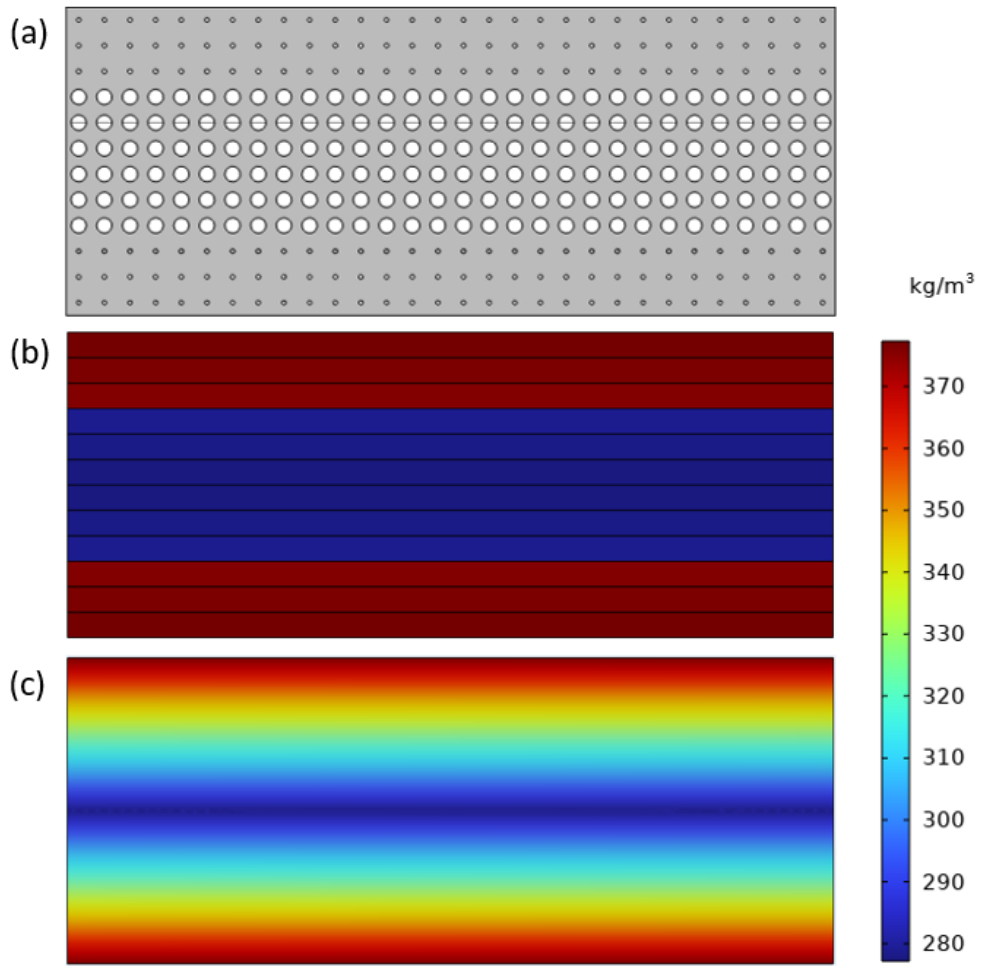

Figure 2.5: (a) Reference plate in longitudinal configuration $k = 0$. (b) Piece-wise constant density equivalent model. Each file is given the exact equivalent density of the corresponding section of the reference model. (b) Linearly varying density equivalent model. The slope and intercept can be freely modified through optimization.

2.3. Finding the equivalent material parameters

As mentioned in Chapter 1, Wood is an orthogonal material and is characterized by nine different elastic parameters as well as its density. Making for ten different and independent parameters that need to be defined. For the reference plates, the considered material parameters are those of Engelman Spruce which was used also in [21]. It is a species of wood often used for soundboards because of its high stiffness and low density. Its material parameters can be taken from the wood handbook [26] which defines the stiffness and shear moduli of various species of wood as well as their Poisson ratios. In particular, the Poisson ratios, density and longitudinal stiffness are listed with a constant value while the other parameters are all given as a ratio to the longitudinal stiffness which can be useful to calculate other material parameters starting from the value of E_L. The ratios from the Wood Handbook as well as the final material properties of the reference plate are listed in Table 2.1.

Material properties	Wood Handbook data	Reference plate
ρ $[Kg/m^3]$	385	385
E_L [GPa]	8.90	8.90
E_R [GPa]	0.128 E_L	1.14
E_T [GPa]	0.059 E_L	0.525
G_{LR} [GPa]	0.124 E_L	1.10
G_{LT} [GPa]	0.120 E_L	1.07
G_{RT} [GPa]	0.010 E_L	0.089
ν_{LR}	0.422	0.422
ν_{LT}	0.462	0.462
ν_{RT}	0.530	0.530

Table 2.1: Material properties of Engelman Spruce.

For the equivalent plates, two different methods are used to calculate the equivalent material parameters and compare their effectiveness in approximating the vibrational behavior of the considered reference plate. The first method consists in applying Caldersmith's formulas using equations 1.1 to calculate E_L, E_R, and G_{LR}, and then use the proportionality coefficients from the wood handbook to calculate the remaining parameters as a function of E_L. This method however doesn't offer a way to calculate the variation of the Poisson ratios of the equivalent plate since they don't depend directly on E_L. The second method relies on optimization of the material parameters to minimize the differences in vibrational properties of the plates and will be explained in detail in the next section.

2.3.1. FEMU optimization and objective function

The optimization of the material parameters of the equivalent plates is implemented on Python using the mph library [40] which allows one to control COMSOL models through it. This brings a lot of flexibility to the optimization process, making it possible to use any optimization algorithm from well known Python libraries, designing a specific objective function, as well as automatizing the whole optimization process.

In particular, the optimization relies on the Finite Element Model Updating method (FEMU). This method, employed in many engineering applications that use a finite element model, aims to calibrate a numerical model based on the actual behavior of a reference structure determined as a part of static and/or dynamic testing of the structure [41]. In this context, it can be applied to calibrate the material parameters of the equivalent plate based on the vibrational behavior of the reference plate. This is done by altering the material parameters of the equivalent plate's numerical model in order to minimize the differences in eigenfrequencies and mode shapes between the two plates. These differences are measured by an objective function L that evaluates these differences using a least squares method. A scheme of this process is summarized in the diagram of Figure 2.6.

First, the target eigenfrequencies and mode shapes of the reference plate are computed numerically on COMSOL using a physics controlled fine mesh and free boundary conditions. Then, initial material parameters are defined for the equivalent plate, and the resulting eigenfrequencies and mode shapes are computed with the same conditions. The results of the reference and equivalent plates are then imported on Python, compared through the objective function, and new material parameters are generated according to the chosen optimization algorithm. These parameters are then sent to the equivalent plate's model on COMSOL and the process is repeated until convergence of the following objective function is reached.

$$L = \sqrt{\sum_i \left(\frac{f_i^R - f_i^{Eq}}{f_i^R} \right)^2} + \alpha \sqrt{\sum_i (1 - MAC_{ii})^2} \tag{2.5}$$

Since it is important to minimize both the differences in eigenfrequencies and in mode shapes to replicate the behavior of the reference plates, the objective function L has two components that are summed and weighted by a coefficient α. The first component measures the error in eigenfrequencies where f_i^R and f_i^{Eq} are the i^{th} eigenfrequency of the reference and equivalent plate respectively. The second component evaluates the

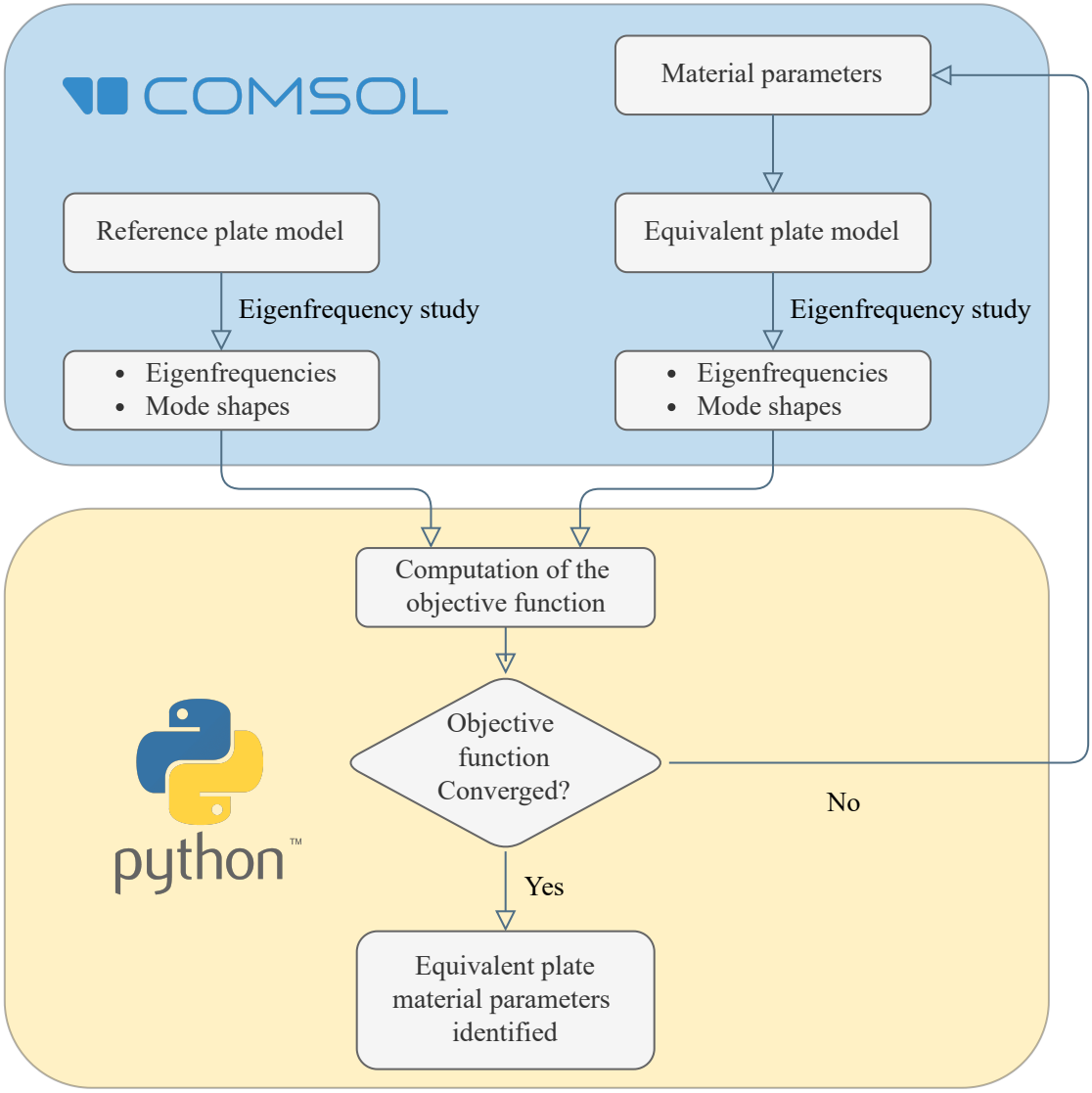

Figure 2.6: FEMU diagram of the optimization of the equivalent plate's material parameters.

error in the modeshapes using the Modal Assurance Criterion commonly called MAC. This criterion is a statistical indicator of the degree of consistency between modeshapes [42, 43] and it takes the form of an $(r \times q)$ matrix.

$$MAC_{r,q} = \frac{|\{\varphi_A\}_r^T \{\varphi_X\}_q|^2}{\left(\{\varphi_A\}_r^T \{\varphi_A\}_r\right)\left(\{\varphi_X\}_q^T \{\varphi_X\}_q\right)}$$

Where $\{\varphi_A\}_r$ is the r^{th} mode of the reference modal vector, and $\{\varphi_X\}_q$ is the q^{th} mode of the equivalent modal vector. This least squares based form of linear regression analysis yields an indicator that is most sensitive to the larger difference between comparative

values, and results in a modal assurance criterion that is relatively insensitive to small changes or small magnitudes. The MAC value can range between 0 to 1, with 1 indicating maximum coherence and 0 indicating completely uncorrelated modeshapes. Figure 2.7a provides an example of an ideal MAC, with values close to 1 along the diagonal, and 0 elsewhere, meaning the reference and equivalent modeshapes would match perfectly.

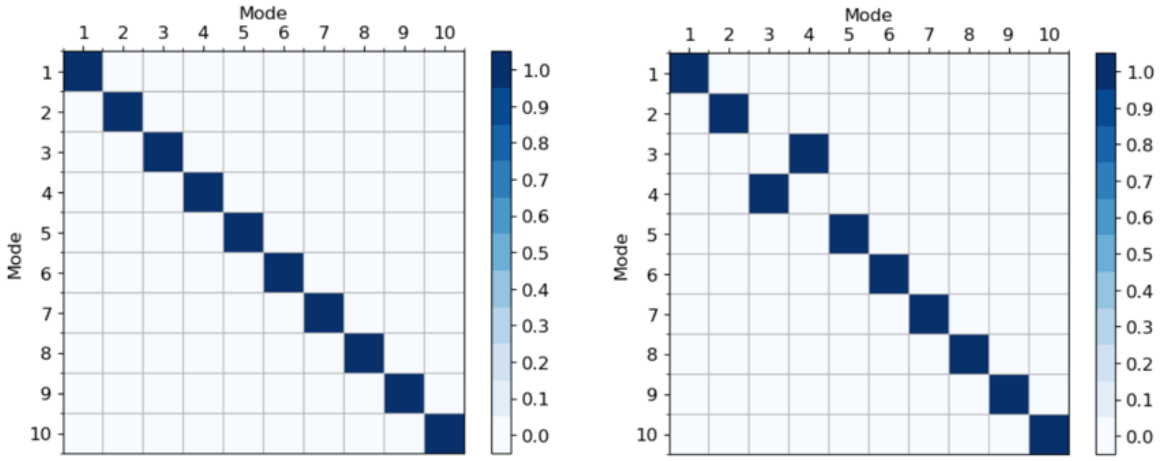

(a) No mode switch (b) Mode switch

Figure 2.7: Two examples of MACs with good correspondence between the first ten mode shapes. The first one presents no mode switches while the second has a mode switch between modes 3 and 4.

When changing the material parameters of an object, the frequency at which each mode of vibration happens is modified unpredictably. Sometimes two modes can have frequencies that are very close together and a modification of the material parameters can cause the order of these modes to be switched in frequency. This phenomenon is called a mode switch. Since the eigenfrequencies and mode shapes exported from COMSOL are always ordered from lowest to highest in frequency, and not by mode, an important part of the optimization script consists in keeping track of eventual mode switches in the equivalent plates in order to compare the correct frequencies in the computation of the objective function. Mode switch tracking is made easy by utilizing the MAC. In fact, as can be observed in Figure 2.7b, a mode switch is easily recognizable in the MAC by the presence of two consecutive values close to 0 in the diagonal, accompanied by two values close to 1 on adjacent off-diagonal cells. This check is done before every evaluation of the objective function and the order of the eigenfrequencies is rearranged accordingly if a mode switch is detected.

2.3.2. Optimization algorithm

The next part of the optimization process regards the choice of optimization algorithm to utilize for the minimization of the designed objective function. Python offers many options from its libraries but for the minimization of a gradient less function such as L, the best choices of algorithms are Nedler-Mead [44] which uses the Simplex algorithm, and Powell's algorithm [45], both from the Scipy library. These two algorithms are not as fast as others which require a gradient of the objective function but they are robust in many applications and can work for the optimization of more than one parameter. Both algorithms have been tested and in the end Nedler-Mead proved to be more efficient for this objective function.

As with many optimization problems, the algorithm can get stuck on a local minima of the objective function and not find the absolute minimum. This is especially true for compound objective functions that have more the one component which is the case with L since it aims to minimize both the difference in eigenfrequencies and in mode shapes. This problem is even more accentuated by increasing the number of parameters that need to be optimized which increases the dimensionality of the problem. To improve this aspect of the optimizations, multiple measures can be taken.

First of all, starting with a good initial guess of the material parameters can help drive the minimization algorithm in the right direction. A first idea could be to start with the material parameters of the reference plate but there are better options. In fact, the Caldersmith formulas can be very helpful for this as they provide already an approximation of the material parameters of the equivalent plate. Another idea could be to use the proportionality coefficients of the Wood Handbook, run a preliminary grid search focused only on finding the optimal value of E_L, and calculating the remaining parameters using said coefficients. This is however a time consuming process which does not particularly improve the results of efficiency of the optimization. Furthermore, the proportionality coefficients do not affect the Poisson ratios meaning their initial guess would not be improved. Because of this, the best initial guess of the material parameters is the one obtained from the Caldersmith formulas.

Another aspect to consider is the definition of boundaries for each parameter that needs to be optimized. Table 2.2 shows the boundaries that have been chosen for the optimization. These boundaries have been selected following an empirical approach, trying different options and choosing the one giving the best results. As can be seen from the table, the restrictions on the parameters are weak for most parameters. Even though it may seem better to restrict the area of research of the parameters to a reasonable range, various

optimization attempts suggest that the algorithm performs better leaving most parameters unrestricted, unless they physically must be within a small range which is the case of the density which cannot be negative, or the Poisson ratios that need to be between 0 and 1. A discussion can be raised about the possibility of having a negative Poisson ratio but it will be addressed in the next chapter. The stiffness and shear moduli parameters on the other hand start with such a high value, which is in the order of Giga-Pascals, that no restrictions are needed for them.

Material properties	Minumum boundary	Maximum boundary
ρ $[Kg/m^3]$	0	None
E_L [GPa]	None	None
E_R [GPa]	None	None
E_T [GPa]	None	None
G_{LR} [GPa]	None	None
G_{LT} [GPa]	None	None
G_{RT} [GPa]	None	None
ν_{LR}	0	1
ν_{LT}	0	1
ν_{RT}	0	1

Table 2.2: Imposed boundaries for the optimization of material parameters.

Finally, some considerations can be made as well about the number of parameters to be optimized. In fact, reducing the number of parameters in the optimization would not only reduce the dimensionality of the problem but also decrease the optimization times. There are methods such as the sensitivity method [46] that aim to find a correlation between the optimization parameters in order reduce their number and simplify the initial problem. This is particularly useful for FEMU problems that tackle complex structures with either a high number of parameters or detailed geometries that require a finer mesh and high computational power for the FEM simulations. In these cases where the numerical simulation alone can take hours, reducing the number of parameters is crucial. Since the geometries of the equivalent plates are simple and can be approximated with good accuracy with coarser meshes, each step of the optimization loop takes only a few second, and thus an order reduction with the sensitivity method was not necessary.

2.3.3. Definition of i and α in the objective function

The last two parameters to calibrate in the objective function of Equation 2.5 are α which controls the weight of the MAC error in the optimization, and i which is the maximum number of eigenfrequencies to consider during the optimization. To find the best value

for these parameters, a trial and error approach is used considering the optimization of the material parameters of the equivalent plate with longitudinal configuration $k = 10$. This is one of the most heterogeneous configurations in Figure 2.2 and as will seen in the Results chapter, it is also one of the hardest configurations to optimize. This particular configuration is used to try the optimization with different values of i and α in order to find their optimal value.

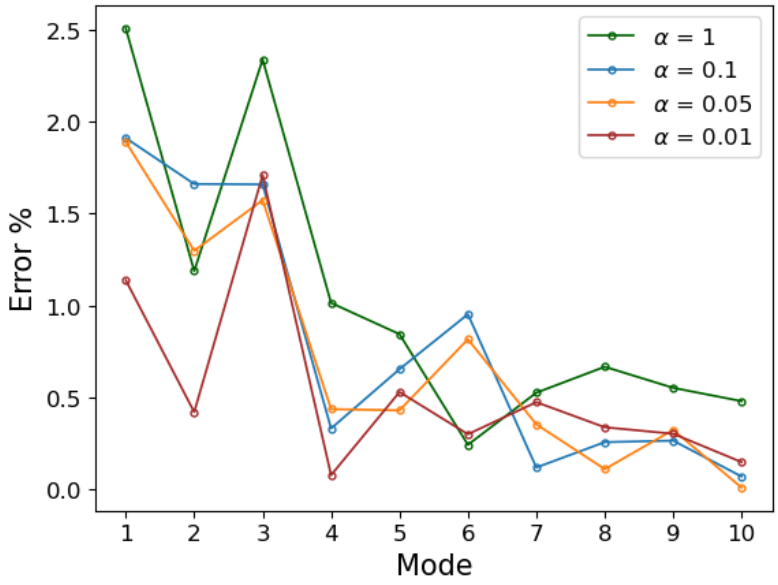

Figure 2.8: Eigenfrequency error between the reference and equivalent models of longitudinal configuration $k = 10$ for different values of α.

Starting with the study of α, Figures 2.8 and 2.9 show the error in the eigenfrequencies and the MAC of the considered equivalent plate for different values of α. In particular, four cases are considered for α being equal to 0.01, 0.05, 0.1, and 1. It is clear that increasing the value of α improves the mode shapes accuracy but increases also the error in the eigenfrequencies of the equivalent plate. A sweet spot can be found nonetheless since only a low value of α is required to improve the MAC as can be seen from Figure 2.9. It can also be observed that lowering the value of α below 0.1 doesn't bring a particularly worthwhile improvement in the accuracy of the eigenfrequencies. Because of that, during all of the subsequent optimizations α will be set at 0.1.

Let us now focus on the identification of the best value for i. The same reference plate configuration is considered, studying this time the first 37 eigenfrequencies and mode shapes which cover the frequency range from 1 Hz up to 1000 Hz to see the effect of i on the higher eigenfrequencies of the plate. Four optimizations of the equivalent plates are ran with i being equal to 10, 15, 20 and 37. Figure 2.10 shows the error in the eigenfrequencies

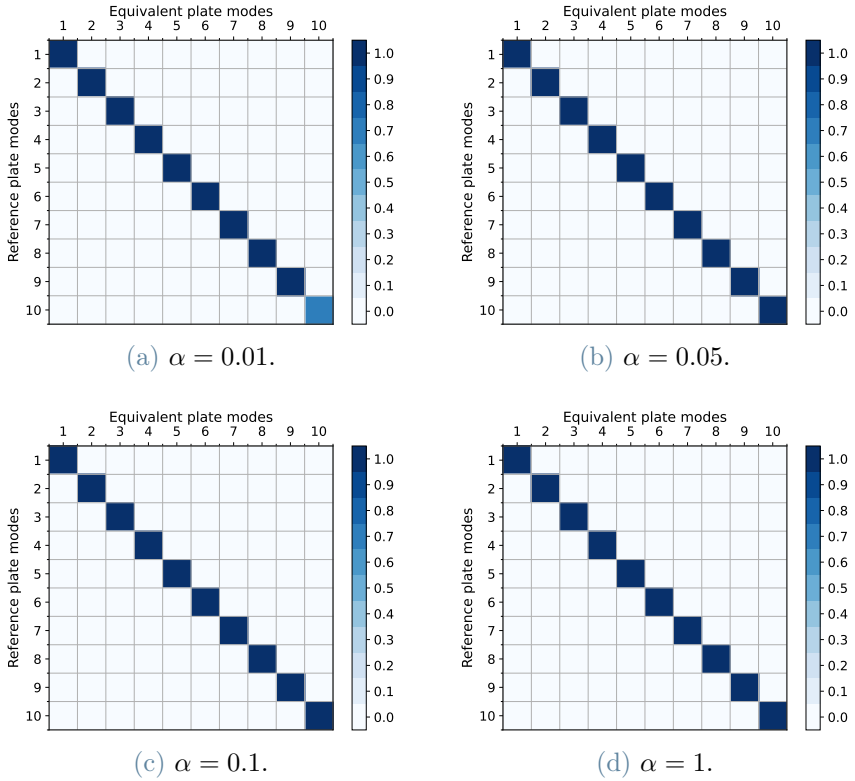

(a) $\alpha = 0.01$. (b) $\alpha = 0.05$.

(c) $\alpha = 0.1$. (d) $\alpha = 1$.

Figure 2.9: MAC for the equivalent plate of longitudinal configuration $k = 10$ for different values of α.

for each value of i. It is clear that if not enough modes are considered in the objective function, the accuracy of the eigenfrequencies can be good at lower frequencies, but the error increases very fast at higher frequencies. It can be seen as well that the accuracy doesn't improve as much for values of i higher than 20. Suggesting that $i = 20$ might be a good compromise between accuracy and computational resources.

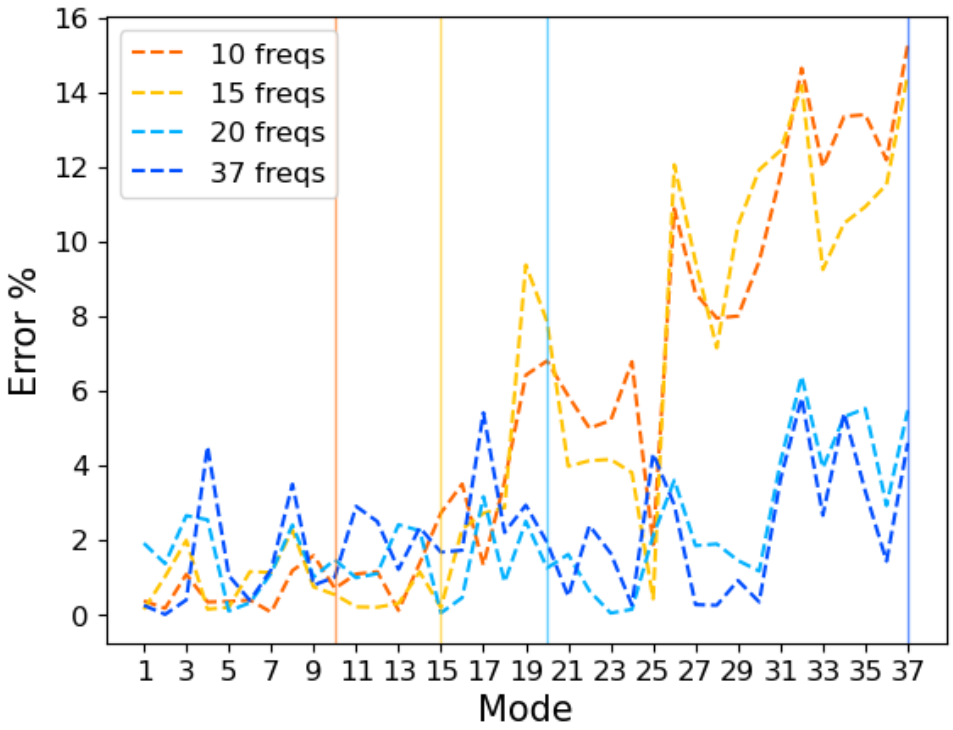

Figure 2.10: Eigenfrequency error between the reference and equivalent models of longitudinal configuration $k = 10$ for different values of i. The vertical lines indicate the last mode considered for each value of i.

Taking a look at the MAC in the cases of $i = 20$ and $i = 37$ in Figure 2.11, it can also be noticed that the mode shapes accuracy at higher frequency does not improve particularly when increasing the value of i from 20 to 37. On the contrary, having a lower value of i brings improvements in the MAC at lower frequencies as can be seen from modes 10, 11 and 12 which are more precise for $i = 20$ than $i = 37$. The value of i used during all optimizations will thus be 20.

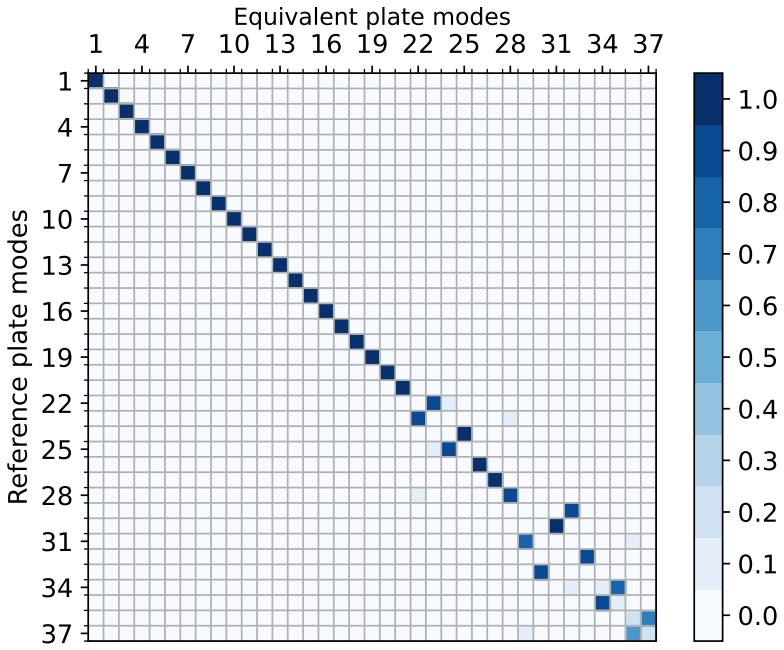

(a) Considering the first 20 modes for the optimization.

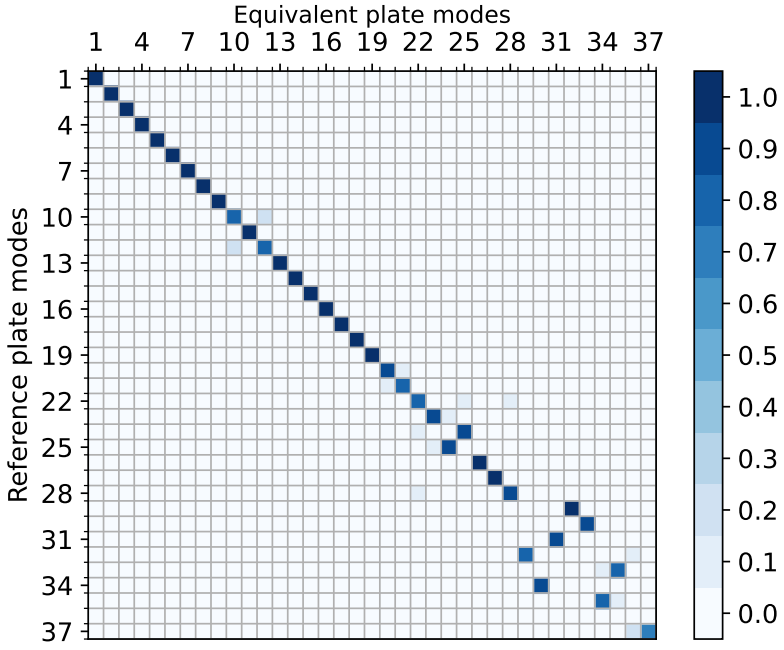

(b) Considering the first 37 modes for the optimization.

Figure 2.11: MAC for the equivalent plate of longitudinal configuration $k = 10$ for different values of i.

3 | Results

The aim of this chapter is to analyze the effects that homogeneous and heterogeneous metamaterial configurations can have on a wooden board. First, the previously described equivalent plate models are used to find out which one can better recreate the vibrational behaviour of the reference for both homogeneous and heterogeneous hole dimension configurations. A comparison is then made to assess the effectiveness of the Caldersmith formulas in the approximation of the elastic constants of the reference plates for heterogeneous metamaterials. Subsequently, the mechanical behaviour of the equivalent plates is analyzed though the application of a static load and compared to that of the reference. A tensile test is carried out as well to investigate the possibility of having a negative Poisson ratio with the most heterogeneous configurations. Finally, the effective material parameters of the equivalent plates are obtained and discussed.

3.1. Equivalent plate of homogeneous hole patterns

Let us consider first the case of the homogeneous hole configuration of the reference plate drawn in Figure 2.1. As mentioned in Section 2.3, its material parameters are those of Engelman Spruce taken from the Wood Handbook [26] which are reported in Table 3.1 for convenience. By performing an eigenfrequency study on COMSOL, the mode shapes and eigenfrequencies of this reference plate can be obtained. An extra fine mesh is used when running simulations on the reference plates in order to get results that are as accurate as possible. The first ten mode shapes and eigenfrequencies of the plates which can be observed in Table 3.2 and Figure 3.1. Our aim is to find an adequate equivalent plate that fits these results as well as possible.

Material properties	Reference plate
ρ $[Kg/m^3]$	385
E_L [GPa]	8.90
E_R [GPa]	1.14
E_T [GPa]	0.525
G_{LR} [GPa]	1.10
G_{LT} [GPa]	1.07
G_{RT} [GPa]	0.089
ν_{LR}	0.422
ν_{LT}	0.462
ν_{RT}	0.530

Table 3.1: Material properties of Engelman Spruce

Mode number	Frequency [Hz]
1	40.0
2	45.7
3	91.6
4	92.6
5	119.5
6	128.5
7	173.6
8	190.8
9	248.4
10	250.8

Table 3.2: First 10 eigenfrequencies of the reference plate

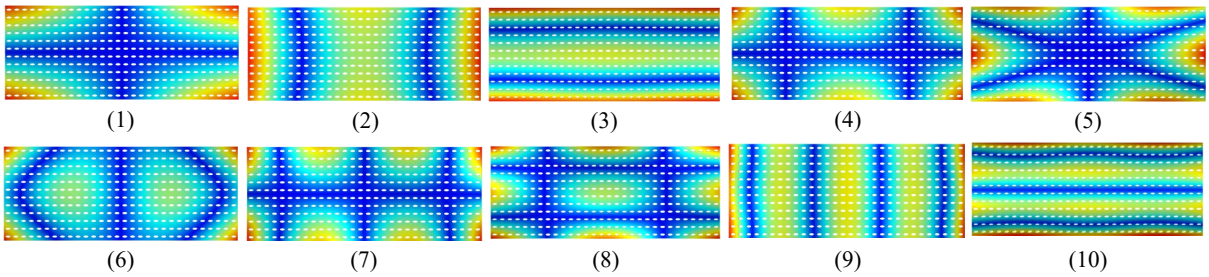

Figure 3.1: First 10 modeshapes of the reference plate. The plots show the displacement for each mode with the nodal lines represented in blue and the points of maximum displacement showcased in red.

In the case of homogeneous hole size distributions, since the density is constant, only the homogeneous model of equivalent plate described in section 2.2.1 is considered. Its material parameters are modified in order to approximate as well as possible the behaviour of the reference plate in terms of modeshapes, eigenfrequencies, and mechanical properties.

We will study first the equivalent plates obtained using the Caldersmith formula approximation, considering the different values of the coefficient used to calculate G_{LR} which are found in literature, and then compare these results with those obtained from the optimization of material parameters.

A first approximation of the material properties of the equivalent plate is obtained through the use of the Caldersmith formulas showcased in section 1.3. In fact, they can be used to approximate the value of the longitudinal and radial Young's moduli E_L and E_R, and the shear Young modulus G_{LR} thanks to equations 1.1 which are reported below. The

remaining material parameters can be approximated using the empirical proportionality coefficients between E_L and the other parameters listed in Table 2.1.

$$\begin{cases} E_L & = 12 \times \dfrac{0.08006\, \rho_{eq}\, a^4\, f_{(0,2)}^2}{h^2} \\ E_R & = 12 \times \dfrac{0.08006\, \rho_{eq}\, b^4\, f_{(2,0)}^2}{h^2} \\ G_{LR} & = 3 \times \dfrac{0.4053\, \rho_{eq}\, a^2\, b^2\, f_{(1,1)}^2}{h^2} \end{cases}$$

In these equations, a and b are the length of the plate along the longitudinal and radial directions respectively, and h is the thickness of the plate. f_{11}, f_{02} and f_{20} are the frequencies of the respective modes of the reference plate which can be identified to be respectively modes (1), (2), and (3) from Figure 3.1. Finally, the equivalent density is calculated as:

$$\rho_{eq} = \rho_{ref}(1 - V_h)$$

Where V_h is the ratio of the volume of the holes with respect to the unit cell and ρ_{ref} is the density of the reference plate.

As previously mentioned in the Background chapter, the expression of G_{LR} can be found with different constants in different research papers. In fact, a coefficient of 0.274 is used by McIntyre in [32] while a coefficient of 0.4053 is used by Caldersmith in [24]. A third possibility is also that of using the proportionality coefficient from the Wood Handbook where G_{LR} is equal to $0.124 \times E_L$. To find out which coefficient is the better approximation for the equivalent plate, an eigenfrequency study on COMSOL is performed calculating the material parameters as in equations 3.1, substituting the value of G_{LR} with each of the three possible options. In particular, the eigenfrequency study is set in the frequency range from $1Hz$ to $1000Hz$ which is the typical range of interest when studying soundboards.

$$\begin{cases} E_L & = 12 \times \dfrac{0.08006\, \rho_{eq}\, a^4\, f_{02}^2}{h^2} \\ E_R & = 12 \times \dfrac{0.08006\, \rho_{eq}\, b^4\, f_{20}^2}{h^2} \\ E_T & = 0.059\, E_L \\ G_{LR} & = X \\ G_{LT} & = 0.120\, E_L \\ G_{RT} & = 0.010\, E_L \\ \nu_{LR} & = 0.422 \\ \nu_{LT} & = 0.462 \\ \nu_{RT} & = 0.530 \end{cases} \tag{3.1}$$

Figure 3.2 shows the error in the frequencies of the first ten modes of the equivalent plate for all three values of G_{lr} as well as an optimized plate which will be commented further below. It can be seen from the plot that the error is lowest when using McIntyre's coefficient. But looking at the MAC plots in Figure 3.3 a few mode switches can be noticed in McIntyre's MAC while the one using the proportionality coefficient is much more accurate. Since the error in the frequencies for the latter coefficient is not much higher than McIntyre's, using the proportionality coefficient from the Wood Handbook will be the preferred way to calculate the value of G_{lr} for the equivalent plates. The material parameters obtained for the equivalent plate through this method are listed in Table 3.3 to be compared with those of the reference plate.

Material properties	Reference plate	Caldersmith's equivalent plate	Optimized equivalent plate
ρ $[Kg/m^3]$	385	327.25	356.08
E_L [Pa]	8.90 E9	6.95 E9	7.50 E9
E_R [Pa]	1.14 E9	7.30 E8	7.49 E8
E_T [Pa]	5.25 E8	4.10 E8	6.39 E8
G_{LR} [Pa]	1.10 E9	8.61 E8	9.04 E8
G_{LT} [Pa]	1.07 E9	8.34 E8	2.93 E8
G_{RT} [Pa]	8.90 E7	6.95 E7	4.48 E7
ν_{LR}	0.422	0.422	0.358
ν_{LT}	0.462	0.462	0.436
ν_{RT}	0.530	0.530	0.715

Table 3.3: Material properties of the reference and equivalent plates

As expected, the stiffness and shear moduli of the equivalent plate are lower than those of the reference plate to compensate for the removal of mass caused by the holes. Figures

3.2 and 3.3 demonstrate that even without optimization, The equivalent plate obtained through the use of Caldersmith's formulas gives a good approximation of the reference plate. In fact, even considering the whole range up to 1000 Hz which covers the first 37 eigenfrequencies, the mean error in the estimation of the eigenfrequencies is of 2.9% and the correspondence of the modeshapes observed in Figure 3.3c is near perfect up to the 30^{th} mode. This is a confirmation that the Caldersmith formulas are effective also on wooden metamaterials with homogeneous hole dimensions.

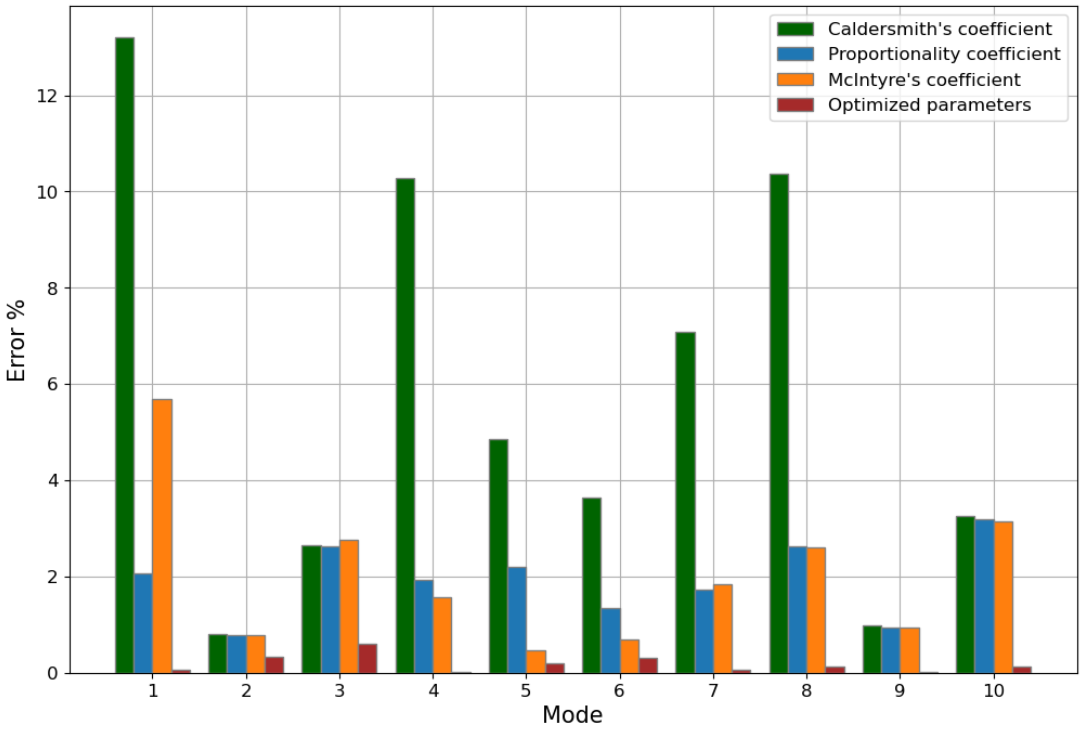

Figure 3.2: Comparison of the error in the first ten eigenfrequencies of the equivalent plates with respect to the reference plate. The first three equivalent plates have the same material parameters except for G_{LR} which is different depending on the used coefficient. For the last one, all of the material parameters are obtained through optimization.

The accuracy of the frequencies and modeshapes of the equivalent plate can however be further improved by optimizing the material parameters using the method described in 2.3. By optimizing the material parameters for the first 20 frequencies and modeshapes of the equivalent plate the mean error in the frequencies is reduced to 0.3%. Additionally, the MAC in Figure 3.3d is near perfect with only two mode switches at the higher frequencies. The material parameters of the equivalent plate obtained through the optimization are also listed in Table 3.3. With respect to the material parameters obtained through the Caldersmith formulas, the variations in the optimized material parameters compared to those of the reference can go from 3% up to 50% but the stiffness and shear moduli still

tend to be lower than those of the reference plate.

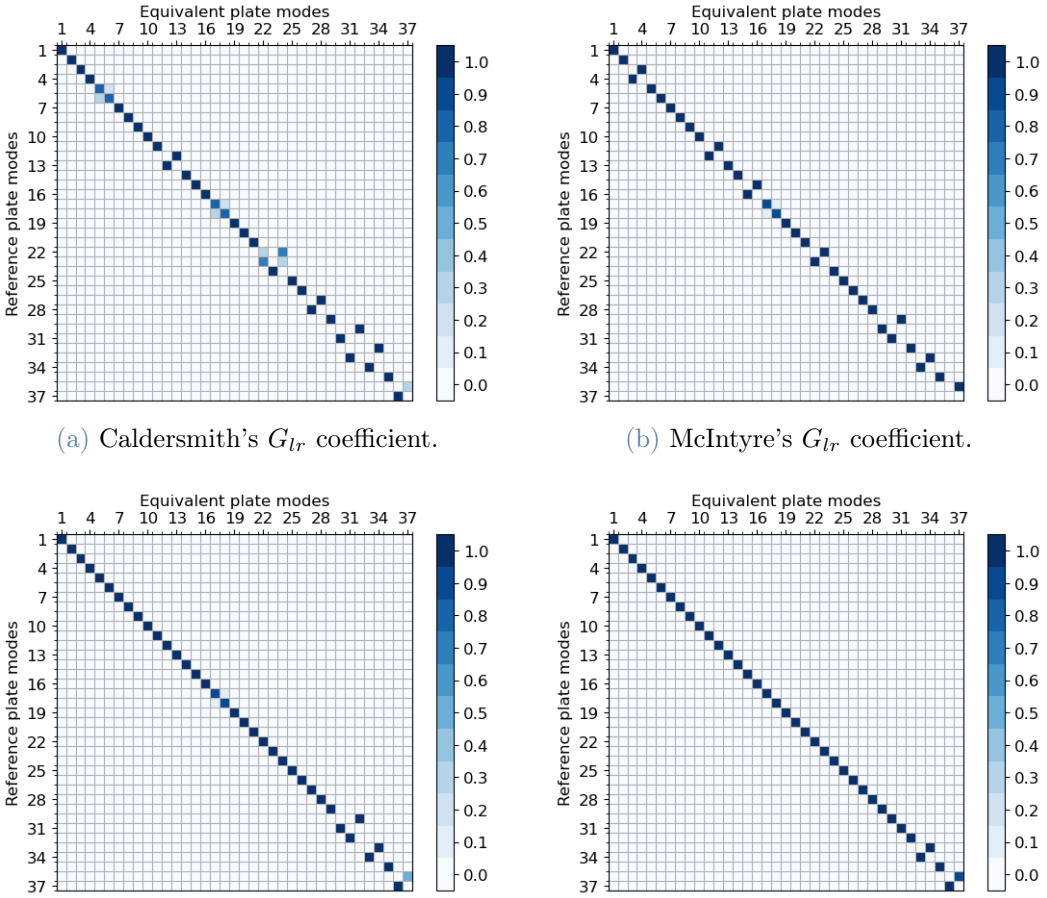

(a) Caldersmith's G_{lr} coefficient.

(b) McIntyre's G_{lr} coefficient.

(c) Wood Handbook's G_{lr} proportionality coefficient.

(d) Optimized material parameters.

Figure 3.3: MAC for the different equivalent plates.

These results indicate that while the Caldersmith formulas can work relatively well in the case of homogeneous configuration the optimization can accurately approximate the material parameters of an equivalent plate with the same eigenfrequencies and modeshapes as the reference up to 1000 $[Hz]$. However, because of the multi-dimensionality of the problem, the obtained parameters are only one of the possible combinations of material parameters that allow the equivalent plate to behave like the reference. Other combinations could be found using different initial material parameters for the optimization. Nonetheless, the obtained parameters can still be considered a good approximation of the effective material parameters of the reference plate.

3.2. Equivalent plates of heterogeneous hole patterns

This section focuses on the study of the 22 heterogeneous configurations described in Figure 2.2. The objective is to first verify the accuracy of the Caldersmith formulas when the density is no longer uniformly distributed on the plate. After that, the optimization algorithm is used on the different equivalent plate models described in section 2.2 in order to find the most accurate approximation of the effective material parameters of the reference plate. Initially, only the error in the eigenfrequencies and modeshapes is considered for each equivalent plate paying no heed to the obtained material parameters since they might not be precise. Once an accurate equivalent plate model has been found, the obtained material parameters will be analyzed trying to effectively find a correlation between different configurations of metamaterials and their effect on the mechanical propertied of the wooden board.

3.2.1. Caldersmith's equivalent plates

First, as with the homogeneous configuration's case, the eigenfrequencies and modeshapes of each reference plate are computed and stored in order to be used as ground truth value for the calculation of the error in the eigenfrequencies and MAC of each considered equivalent plate model. Then, using the homogeneous density equivalent plate model, the eigenfrequencies and modeshapes of each heterogeneous configuration are computed using the material parameters obtained from the application of the Caldersmith formulas following the same approach as in the previous section. Figure 3.4 shows the mean and standard deviation of the relative error of the computed eigenfrequencies with respect to the reference for each mode over all 11 configurations k. The longitudinal symmetry configurations are separated from the radial symmetry ones for comparison clarity.

It is evident that the standard deviation is pretty large for most modes when using the Caldersmith method, especially for the configurations with radial symmetry. The only exceptions are the second and fourth mode which correspond to modes $(0, 2)$ and $(2, 0)$. These are the modes used in the Caldersmith formulas in Equation 3.1 to tune the plate to these frequencies and indeed the standard deviation as well the mean error are particularly low for these two modes. This shows that Caldersmith's formulas are very precise in tuning the wooden boards at these specific frequencies but are not as effective for the remaining frequencies in the case of heterogeneous hole dimensions in the metamaterial. Another observation that can be made from this figure is that configurations with radial symmetry have a higher error with respect to the ones with longitudinal symmetry. Perhaps because having a varying distribution of hole dimensions along the longest side of the plate has a

greater effect on its material parameters.

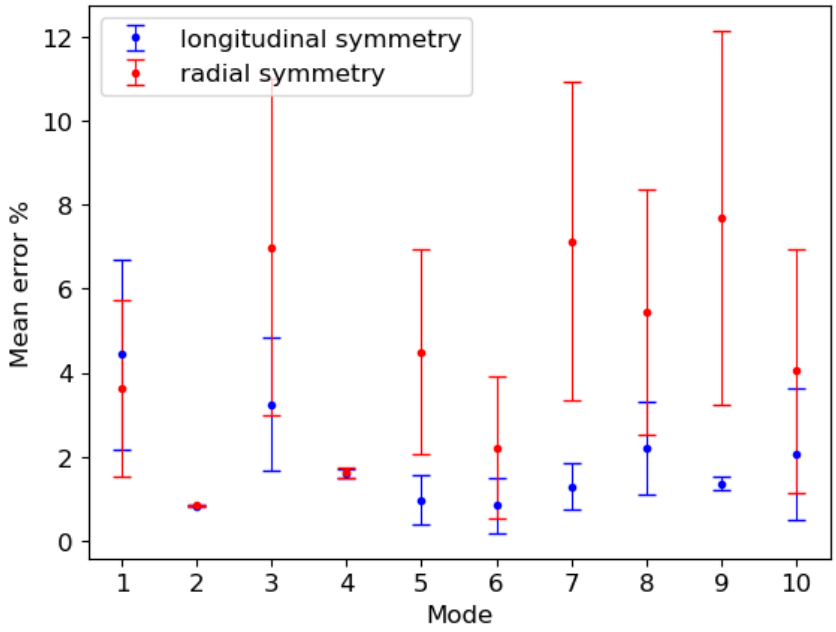

Figure 3.4: Mean and standard deviation of the eigenfrequencies error. A comparison between the longitudinal and radial symmetry configuration equivalent plates obtained via the Caldersmith method.

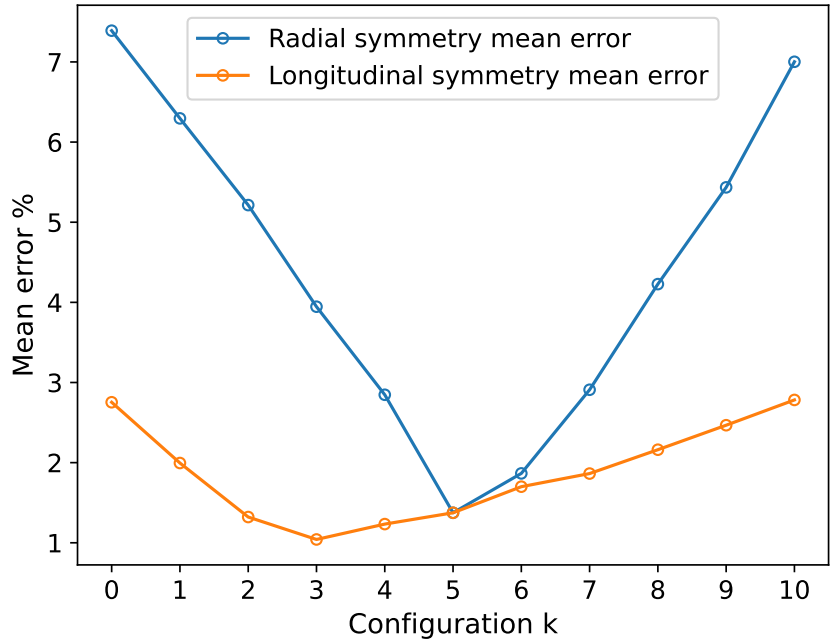

Figure 3.5: Mean error of the first 10 eigenfrequencies calculated for each configuration for both radial and longitudinal symmetry cases.

In Figure 3.5, the mean error computed over the first 10 eigenfrequencies is plotted for each configuration k. Here, remembering that configurations 0 and 10 are the most heterogeneous in terms of hole dimensions while configuration 5 corresponds to the homogeneous case, it is clear that the approximation of the material parameters given by the Caldersmith formulas works best for more homogeneous configurations, but cannot be considered accurate for heterogeneous distributions of the mass on the plate. Again, it is evident that radial symmetry configurations have a higher error than the ones with longitudinal symmetry.

Taking a closer look at the error in the eigenfrequencies for each different configuration in radial symmetry, Figure 3.6 reveals that the minimum error is reached for configuration 5. On the other hand, the error gets gradually higher while getting closer to configurations 0 and 10 with an error going as high as 16% for the ninth mode of configuration $k = 10$.

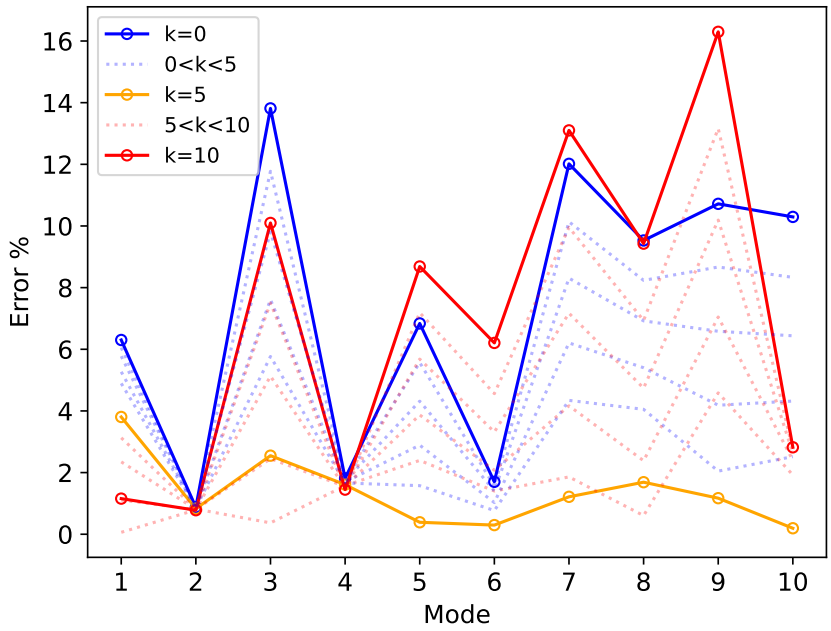

Figure 3.6: Frequencies error of all radial configurations for the first 10 modes. The error is at its minimum for the homogeneous configuration k = 5.

This discrepancy in the accuracy of the equivalent plates can be observed also examining the MAC of these configurations. Figure 3.7 shows the mean MAC of the first 10 modes computed over all radial and longitudinal configurations separately. In general, there is a good correspondence of the modeshapes in both cases. The least accurate matching happening for modes 5, 6 and 10 in radial configurations.

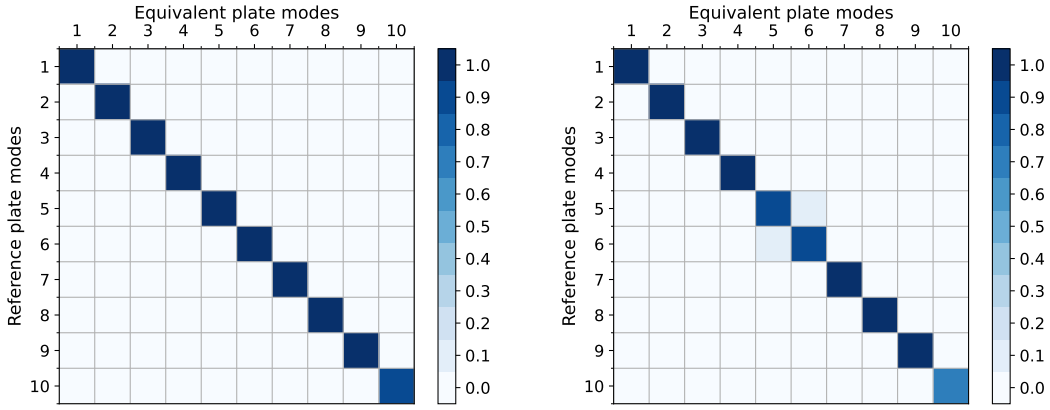

(a) Longitudinal configurations. (b) Radial configurations.

Figure 3.7: Mean MAC of all configurations for longitudinal and radial symmetry.

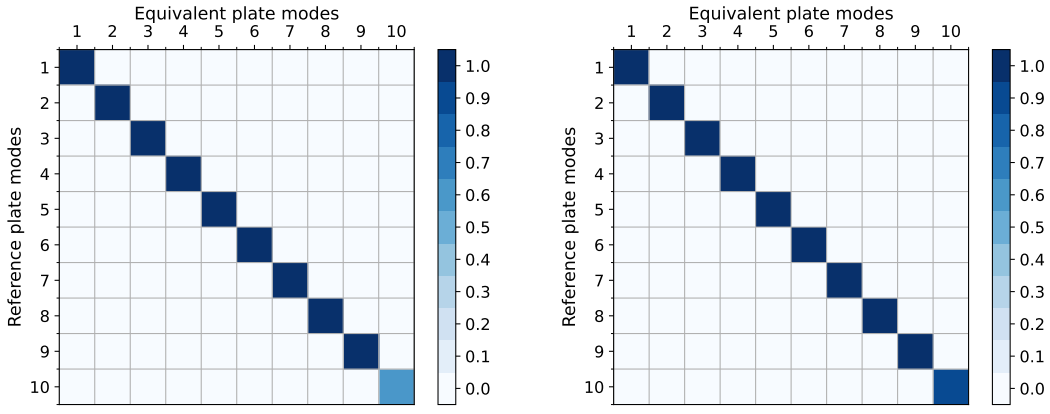

(a) k = 0. (b) k = 5.

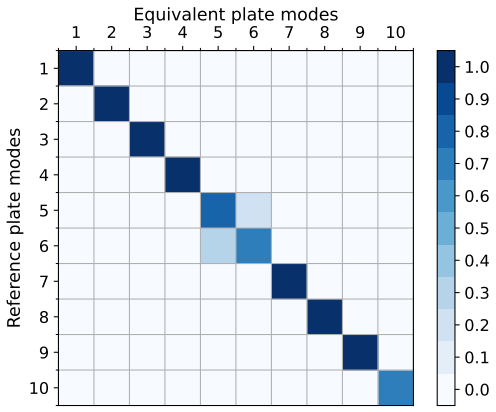

(c) k = 10.

Figure 3.8: Mac of configurations 0, 5 and 10 with radial symmetry.

More specifically, by analyzing the MAC of each single configuration it can be noticed that the error is more pronounced in the most heterogeneous configurations. In fact, Figure 3.8 shows that while the MAC is very accurate for configuration $k = 5$, configuration 0 reveals an inconsistency with mode 10 while configuration 10 shows some confusion with modes 5 and 6.

Figure 3.9 shows these last two modes for both the reference and equivalent plate for radial configuration $k = 10$. It can be seen that while the represented modes are still recognizable in both plates as mode (0,3) for mode 5 and mode (2,1) for mode 6, the nodal lines further from the radial axis of symmetry of the plate are slightly bent. A similar effect is observed for mode 10 as well.

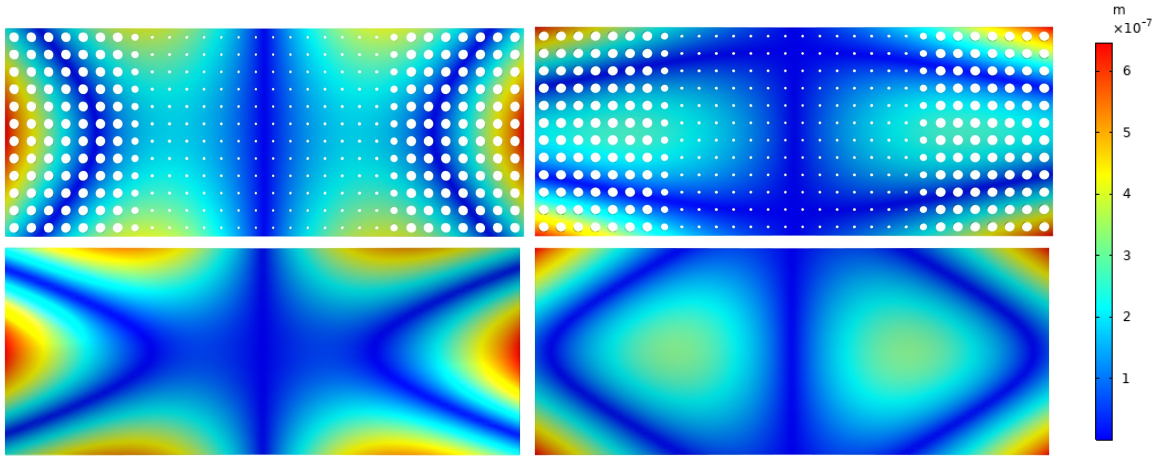

Figure 3.9: Displacement plots for modes 5 on the left hand side, and 6 on the right hand side. On the top side is reference plate in configuration k = 10 with radial symmetry, and on the bottom side is its equivalent plate.

3.2.2. Influence of Poisson's ratio on the modeshapes

Before moving on to the study of the optimized equivalent plate, let us investigate the cause behind the bending of nodal lines in some modes. Considering the equivalent plate obtained in the previous section for radial configuration k = 10, multiple simulations are ran on COMSOL keeping all material parameters fixed except for one. This free parameter is made to vary between a selected range in order to verify its effect on mode shapes 5 and 6. Repeating this process for all the material parameters of the equivalent plate, it can be found that the bending of nodal lines is caused mainly by the Poisson ratio ν_{LR}. In fact, making this coefficient vary from -1 to 1 can produce a range of variation in the mode shapes, especially in the range between - 0.5 and 0.5 as can be seen from Figure

3.10.

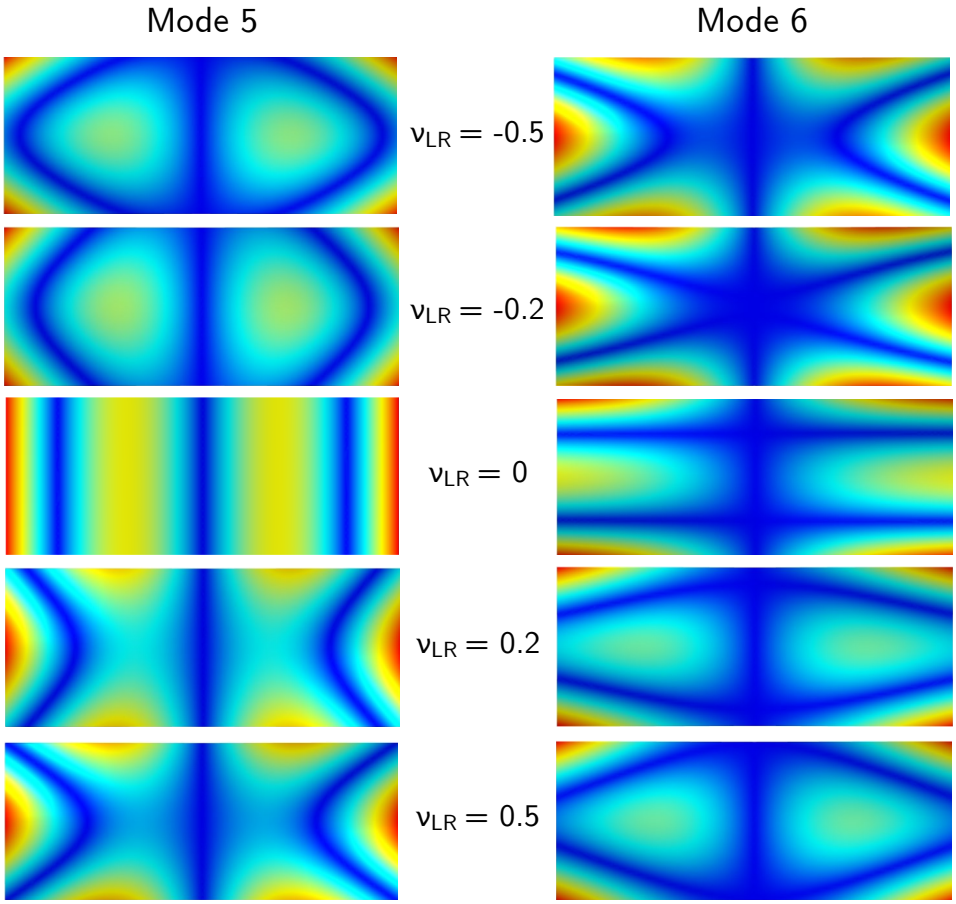

Figure 3.10: Variation of modeshapes 5 and 6 for radial configuration k = 10 for different values of v_{LR} while keeping the remaining material parameters constant.

As mentioned previously, only the nodal lines outside from the central radial axis of symmetry of the plate are affected by the bending. Another observation to be made is that the conventional shape of modes (0,3) and (2,1) are obtained for $v_{LR} = 0$. Variations of the coefficient in positive or negative directions cause the bending of the nodal line in opposite directions. This effect is much less pronounced in other modes but still noticeable. If studied more, this could prove to be an interesting way to manipulate the mode shapes of a wooden board.

3.2.3. Optimized equivalent plates

Since the equivalent plates simulated using the Caldersmith formulas do not give a good enough approximation of the material parameters for heterogeneous configurations, the optimization method is used to try to find a better equivalent model of the reference plates. To this aim, this section analyzes the results obtained from the optimization of the material parameters of each of the equivalent plate models described in section 2.2. That is to say the homogeneous density model which was used for the Caldersmith formulas method in the previous section, the variable thickness model, and the two variable density models. For each of these cases, the simulations are performed on the most heterogeneous configurations in order to see if their error can be improved.

Homogeneous equivalent plate model

Taking as reference the four most heterogeneous configurations, namely configurations 0 and 10 for both longitudinal and radial symmetry patterns, an optimization of the material parameters is performed on the homogeneous density equivalent model for each of them. The relative errors between the obtained eigenfrequencies and their respective reference plate's eigenfrequencies are calculated and compared to the error calculated for the previous Caldersmith formulas equivalent plates. Figure 3.11 shows the mean error over the four considered configurations for the optimized equivalent plates and the ones obtained through the Caldersmith method.

Considering the first ten modes of vibration, the error is effectively reduced when applying an optimization of the material parameters. In fact, the mean error over the first ten eigenfrequencies is reduced from 4.98 % with the Caldersmith formulas equivalent plates to 2.67 % with the optimization.

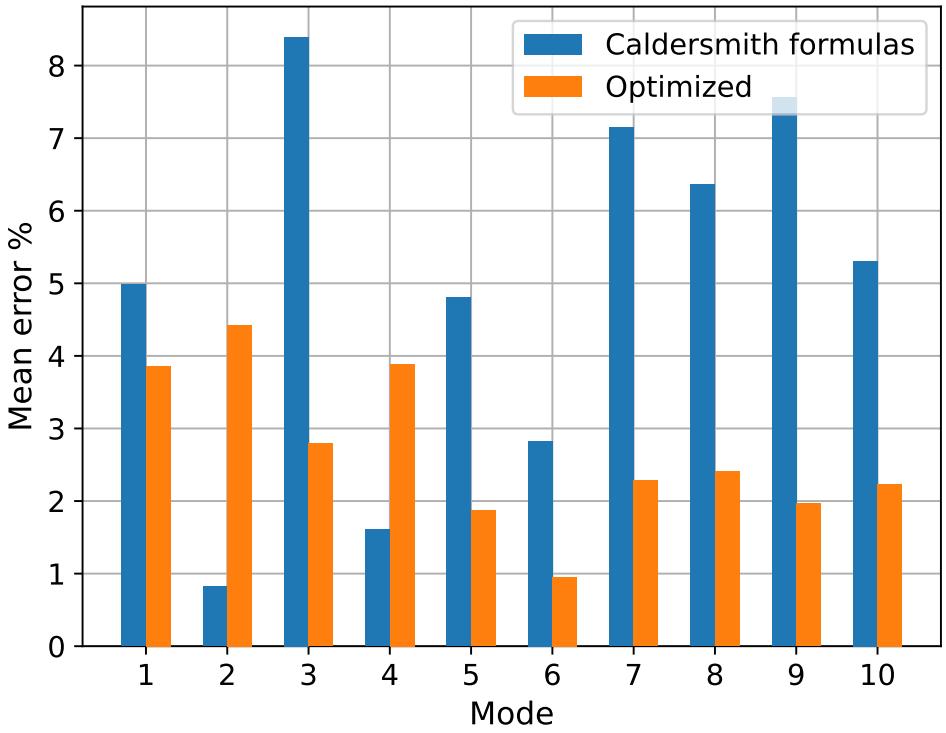

Figure 3.11: Mean error of the first ten eigenfrequencies computed over configuration 0 and 10 for both longitudinal and radial symmetry. The mean is calculated for the eigenfrequencies obtained from the optimization and compared with the mean error obtained from the previously calculated Caldersmith formulas equivalent plates.

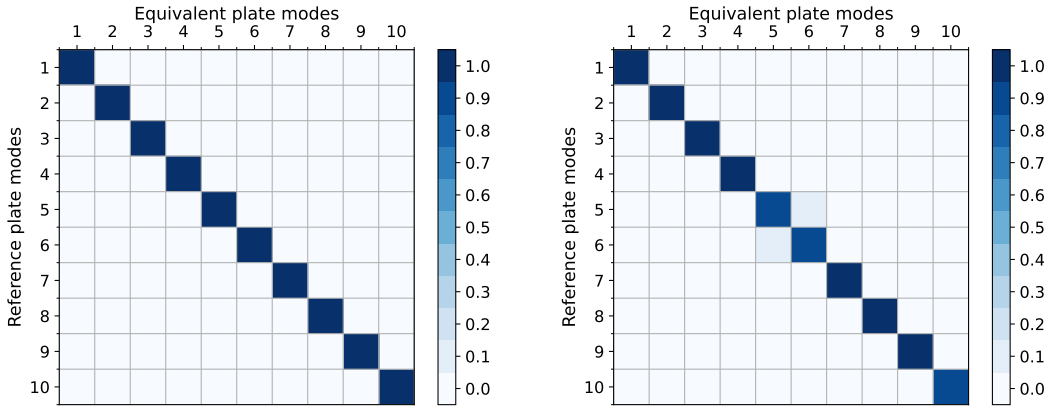

(a) Longitudinal configurations. (b) Radial configurations.

Figure 3.12: Mean MAC of configurations 0 and 10 for longitudinal and radial symmetry.

The MACs shown in Figure 3.12 show a little improvement in the precision of the first ten mode shapes using the optimization although a slightly lower value can still be noticed

for modes 5 and 6.

The optimization improved the accuracy of the eigenfrequencies and mode shapes of the equivalent plate for the most heterogeneous configurations but has reached a limit. In fact, using an equivalent model with constant density fails to capture the different distribution of mass on the plate caused by holes of varying dimensions and thus, an accurate recreation of the vibrational behaviour of the reference is difficult.

Variable thickness and density models

The equivalent plate models studied in this section are designed to take into account the mass variation in heterogeneous configurations by changing either the thickness or density distribution in the equivalent plate. In order to verify the effectiveness of each model, the approach considered in the previous section is applied. In particular, since the behaviour of the four most heterogeneous configurations is similar, the results will be shown only for configuration 0 with longitudinal symmetry for clarity.

First, considering the variable thickness model described in section 2.2, equation 2.2 is used to calculate the height at the center of each cell and the thickness profile of the plate is drawn using COMSOL's interpolation function. The resulting profile of longitudinal configuration 0 is drawn in Figure 3.13. The material parameters of this equivalent plate are optimized and the resulting eigenfrequencies will be compared with the ones from the other models in Figure 3.16.

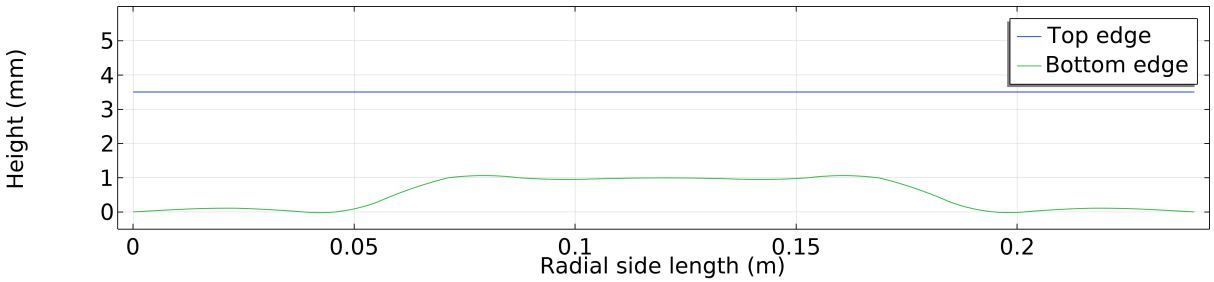

Figure 3.13: View in the **RT** plane of the variable thickness height profile for longitudinal configuration 0.

The second model studied is the one with piece-wise constant density described in section 2.2 and shown in Figure 2.5. In this case, the geometry of the equivalent plate has the same length, width and thickness as the reference plate. Its density however is modified by calculating the equivalent density of each file (i) of holes from longitudinal configuration 0 using equation 2.3.

$$\rho_{eq}(i) = \rho_{ref}\left(1 - \frac{\pi R(i)^2}{l^2}\right)$$

The resulting density distribution on the plate is shown in Figure 3.14.

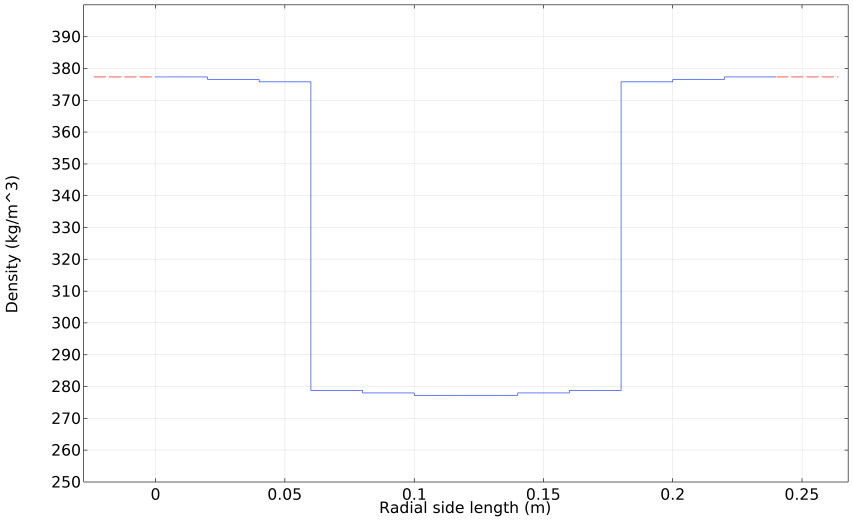

Figure 3.14: Piece wise constant density for longitudinal configuration 0.

Until now, The optimization algorithm has been applied using 10 parameters as arguments. Namely, the 9 mechanical elastic parameters and the density. Because this model has 6 different values for the density, considering that the last 6 values are identical to the first 6 due to the symmetry of the plate, the optimization of material parameters is done considering only the 3 Young moduli, 3 Shear moduli, and 3 Poisson ratios in order to avoid unnecessarily increasing the dimensionality of the problem.

The last equivalent model considered is the one with linear variation of the density described in section 2.2. Its geometry is the same as the previous equivalent plate model but its density is instead approximated by the linear function of equation 2.4 which is reported below.

$$\rho_{eq}(x) = dx + \rho_0$$

In this case, the density distribution is described by two variables; The slope d and the intercept ρ_0. That being so, including the density in the optimization only increases the number of parameters to be optimized by one making it possible to optimize for the density as well with this equivalent model. The initial values of a and ρ_0 are calculated by applying equation 2.3 as:

$$\rho_0 = \rho_{eq}(1) = \rho_{ref}\left(1 - \frac{\pi R(1)^2}{l^2}\right)$$
$$d = \frac{\rho_{eq}(6) - \rho_0}{b/2}$$

Where ρ_0 is equal to the equivalent density of the first row of holes $\rho_{eq}(1)$ and d is calculated as the slope between the density of file 1 and that of file 6. b being equal to the length of the plate in the radial direction. The obtained density distribution is plotted in Figure 3.15.

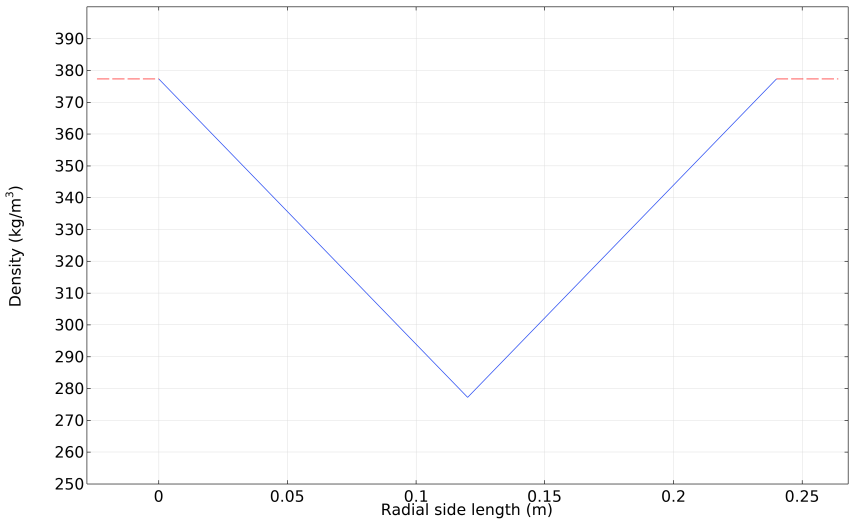

Figure 3.15: Linear density for longitudinal configuration 0.

Using the data obtained from the optimization of each of the previously equivalent models, the errors in the first ten eigenfrequencies are computed and compared to each other in Figure 3.16.

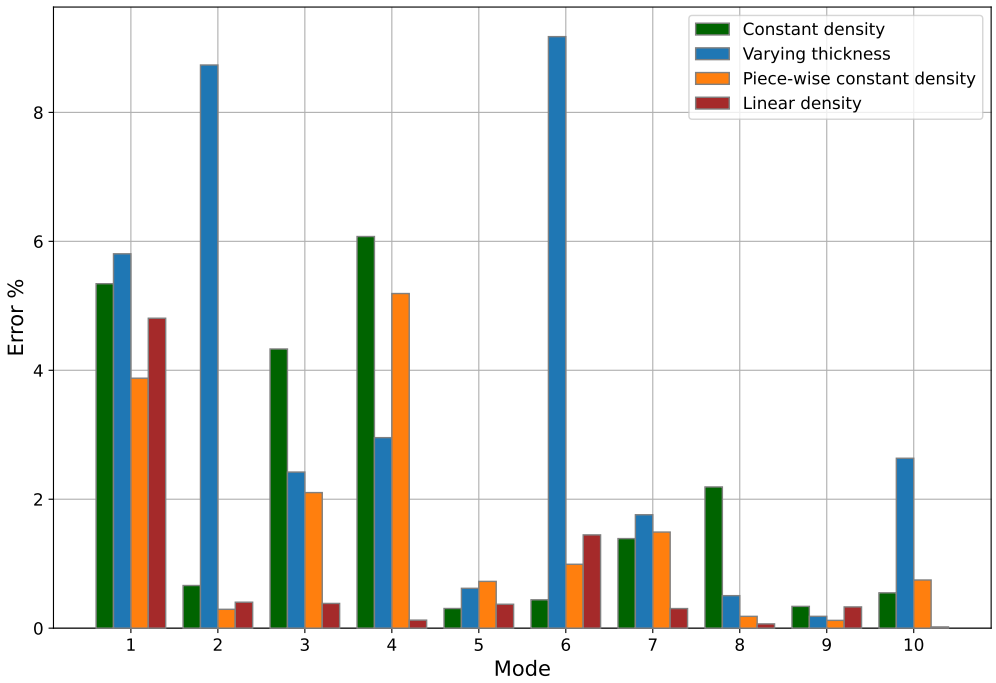

Figure 3.16: Comparison of the eigenfrequency errors for the optimized models with constant density, varying thickness, piece-wise constant density, and linear density, for the longitudinal symmetry configuration 0.

Upon initial observation, it is evident that not all the equivalent models improve the results of the first constant density model. In fact, the error is generally higher when using a varying thickness model. Suggesting that modifications to the geometry of the plate significantly alter its vibrational behaviour and makes it difficult to match the eigenfrequencies even after optimization of the material parameters. The varying density models on the other hand offer a substantial improvement in the accuracy of the eigenfrequencies. Especially the one using a linear variation of the density which reduces the mean error on the first ten eigenfrequencies from 2.67 % to 0.83 %, a value that is even lower than experimental error.

This model is thus used concurrently with the optimization of material parameters in order to obtain the equivalent plates of all heterogeneous configurations.

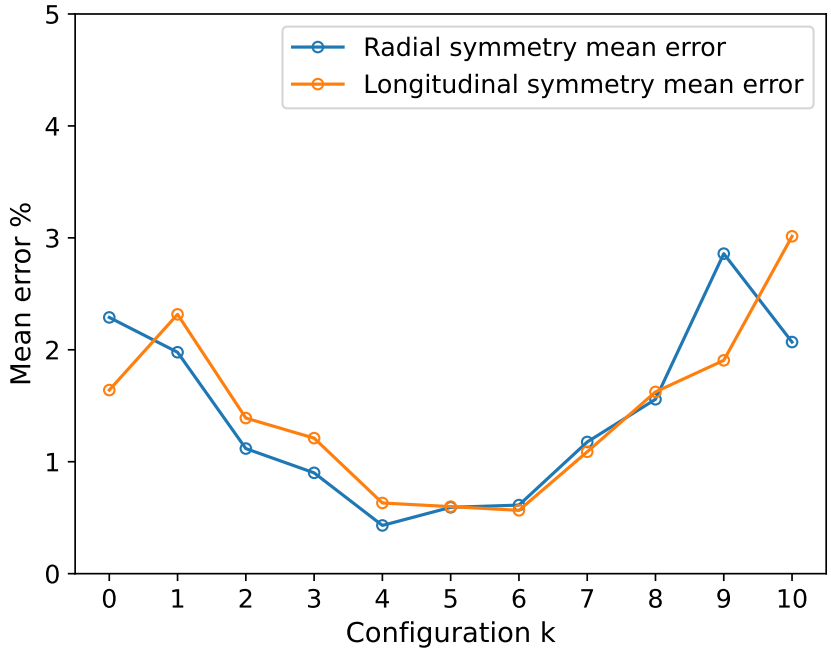

Figure 3.17: Mean error of the first 37 eigenfrequencies calculated for each optimized configuration for both radial and longitudinal symmetry cases.

Figure 3.17 shows the mean error computed over the first 37 eigenfrequencies for each configuration k, separating longitudinally symmetric configurations from the radially symmetric ones. Compared to Figure 3.5 which showed the error of the equivalent plates obtained from the Caldersmith method, and where the error was computed over the first 10 eigenfrequencies instead of 37, the mean error is drastically reduced. Especially for the radial symmetry configurations. In fact, while a much higher error was noticed for the most heterogeneous radial configurations using the Caldersmith method, the error of the eigenfrequencies with the linear density variation equivalent model is kept low and is similar for both radially and longitudinally symmetric configurations.The total mean error of all configurations being equal to 1.43 %.

It is interesting to notice that even with an equivalent plate specially designed to take into account the mass variation caused by heterogeneous configurations of holes, the error is still slightly higher for the most heterogeneous distributions compared to the homogeneous case. This goes to show that the more heterogeneous as configuration is, the more its behaviour differs from that a of a solid plate. Furthermore, the ability to tune the eigenfrequencies of a plate through the application of a specific pattern of holes is a promising result which when further developed, could be used in instrument making where certain modes are believed to correlate with the acoustic performance of the instrument.

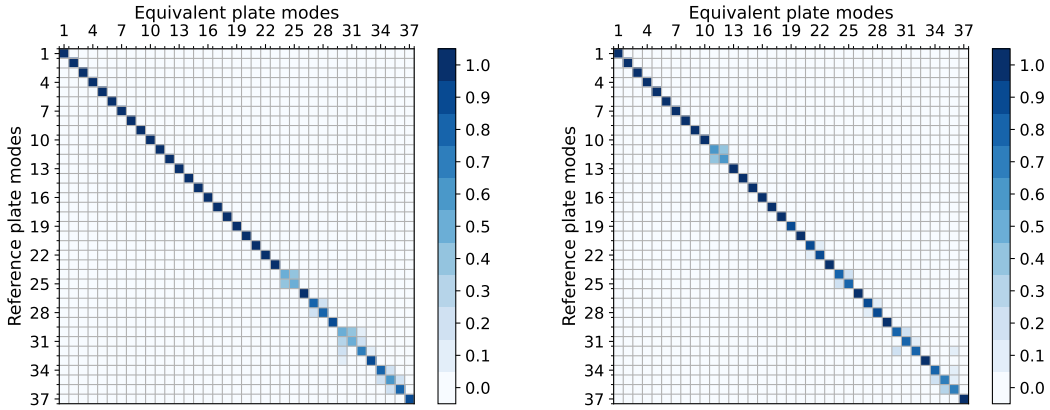

(a) Longitudinal configurations. (b) Radial configurations.

Figure 3.18: Mean MAC of all configurations separated for longitudinal and radial symmetry considering the first 37 modes.

The MAC matrices displayed in Figure 3.18 show that on top of being able to match the eigenfrequencies of the reference plates with a low error, the proposed equivalent plate model recreates with good precision most mode shapes up to the 37th mode. As a result, the equivalent plates obtained through the optimization of the material parameters of the linear density model will be the ones considered in the studies of the following sections.

3.3. Static analysis of the obtained equivalent plates

Studying the eigenfrequencies and mode shapes of the reference and equivalent plates allowed for an accurate reproduction of the vibrational behavior of the reference plates through a dynamic analysis. This section aims to verify the mechanical behavior of the obtained equivalent plates by submitting them to a static analysis. More particularly, this is done in COMSOL by applying a stationary distributed load of 10 N on the surface of the plate lying in the **LR** plane while a fixed boundary condition is applied on two parallel sides at a time. Either the ones parallel to the **LT** plane or the ones parallel to the **RT** plane. Subsequently, the Von Mises stress caused by this load is computed for both reference and equivalent plate, and the displacement of the plate in the same direction of the applied force is measured and compared in the two cases as well.

3.3.1. Von Mises stress and plate's displacement

Let us consider first the case of homogeneous configuration $k = 5$. Figure 3.19 shows the Von Mises stress caused by a distributed 10 [N] force applied in the tangential direction while the longitudinal sides of the plate are fixed. Right below it, Figure 3.20 illustrates the displacement of the radial edges of the plates still in the tangential direction.

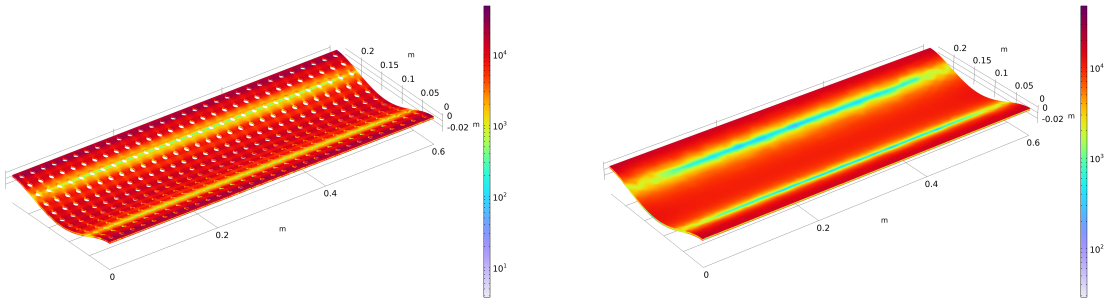

(a) Reference plate. (b) Equivalent plate.

Figure 3.19: Von Mises stress $[N/m^2]$ measured on the homogeneous configuration with k = 5 for a 10 [N] distributed force applied on the top surface of the plate. Fixed boundary conditions are applied on the longitudinal sides of the plate.

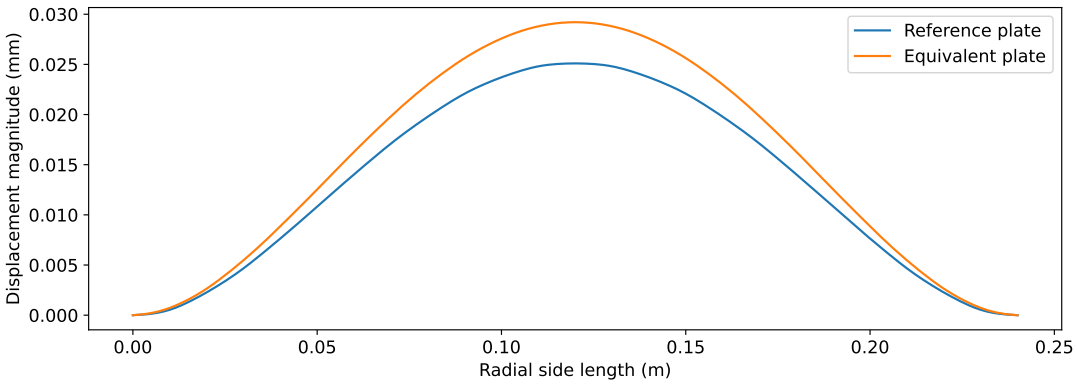

Figure 3.20: Displacement of the radial edges in the tangential direction on configuration k = 5.

The distribution of the Von Mises stress on the reference and equivalent plates shows a good similarity between the two. Small disturbances can be noticed in the equivalent plate near the radial edges although they are likely just an artifact of the meshing process. Looking at the displacement of the radial edges in both plates, the two are very similar with the maximum displacement observed in the equivalent plate being higher by

approximately 0.002 mm which is a negligible quantity. A good correspondence is thus found between the mechanical behaviour of the reference and equivalent plates in the case of the homogeneous metamaterial configuration.

Considering instead one of the most heterogeneous configuration, namely configuration 10 in the case of longitudinal symmetry, the same experiment is repeated twice applying the fixed boundary conditions first to the longitudinal sides as was done in the previous case, and then to the radial sides of the plate. Figures 3.21 to 3.24 show the results for both tests.

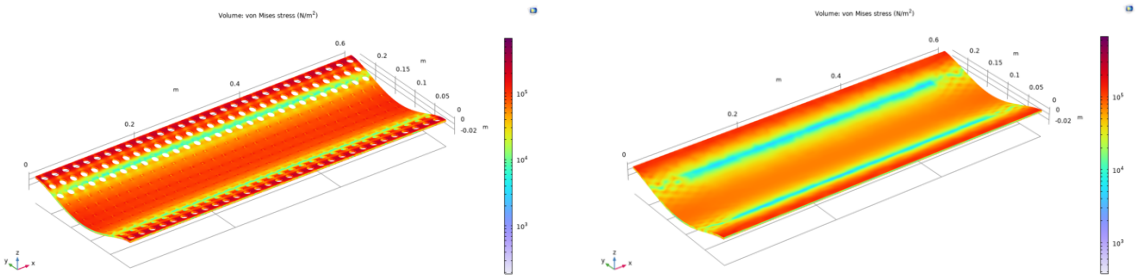

(a) Reference plate. (b) Equivalent plate.

Figure 3.21: Von Mises stress $[N/m^2]$ measured for configuration k = 10 with longitudinal symmetry for a 10 [N] distributed force applied on the top surface of the plate. Fixed boundary conditions are applied on the longitudinal sides of the plate.

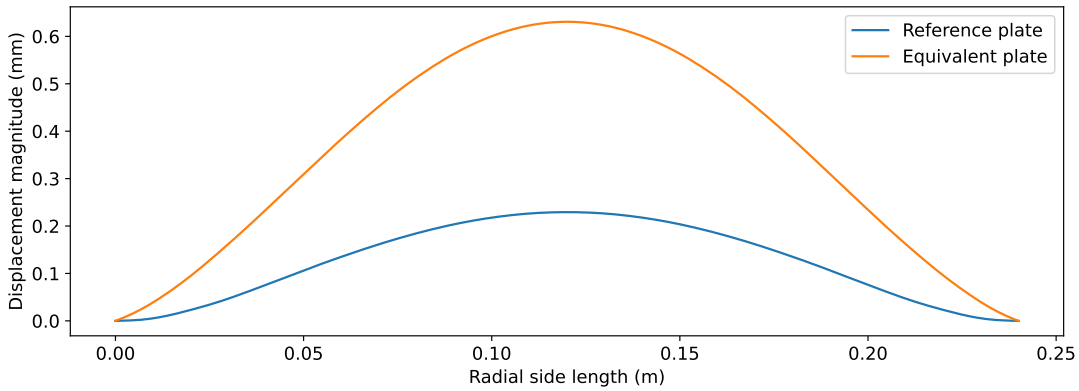

Figure 3.22: Displacement of the radial edge in the tangential direction for longitudinal configuration k = 10.

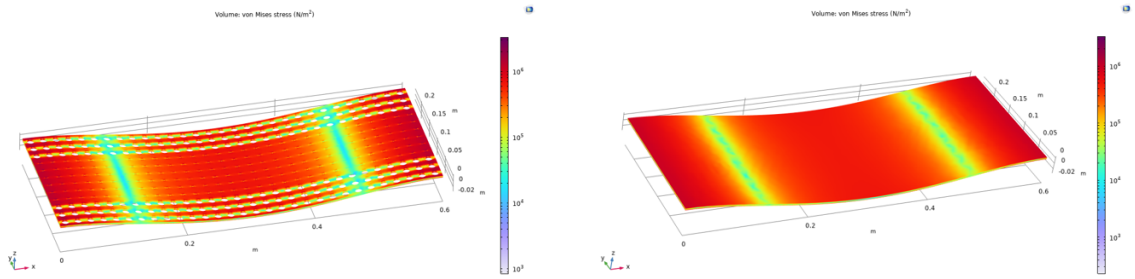

(a) Reference plate. (b) Equivalent plate.

Figure 3.23: Von Mises stress $[N/m^2]$ measured for configuration k = 10 with longitudinal symmetry for a 10 [N] distributed force applied on the top surface of the plate. Fixed boundary conditions are applied on the radial sides of the plate.

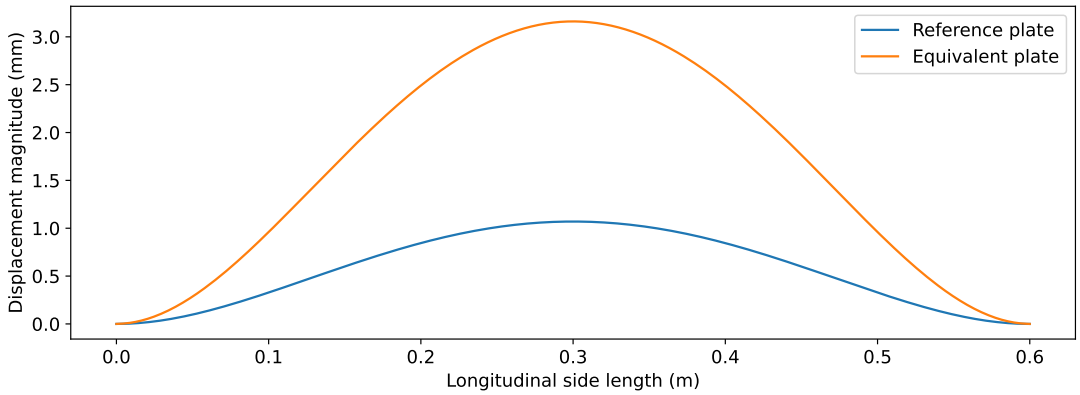

Figure 3.24: Displacement of the longitudinal edge in the tangential direction for longitudinal configuration k = 10.

Just as with the homogeneous configuration, there seems to be a good matching between the Von Mises stress on the reference and equivalent plates in both cases of boundary conditions. The displacement plots however reveal that for the same force applied on the plates, different magnitudes of the displacements are obtained. In fact, the maximum magnitude of the displacement of the equivalent plates is approximately 3 times higher than that of their respective reference. The effective difference is of 0.4 mm in the first case and 2 mm in the other which is a noticeable change considering that the thickness of the plate is of 3.5 mm. This behaviour has been observed with other configurations as well although with less difference between the maximum displacements of the reference and equivalent plates. The largest difference having been obtained for longitudinally symmetric configuration 10 shown in the figures.

These results indicate that the calculated stiffness of the equivalent plates is slightly lower

than the effective stiffness of their respective reference which causes a larger displacement for the same applied force. Revealing thus a discrepancy between the results of the dynamic analysis conducted in the earlier sections and the static study conducted here, especially for the most heterogeneous metamaterial configurations. This difference in the behaviour of the equivalent plates when subjected to a dynamic analysis versus a static one is an interesting effect which could be used in the future to design bespoke instruments.

3.3.2. Measuring the Poisson ratio with a tensile test

In the definition of the material parameter boundaries for the optimization in Table 2.2, the Poisson ratios have all been set with a minimum value of 0 and a maximum value of 1. This range is reasonable for common materials but some particular metamaterials are known to exhibit auxetic behaviors such as the one represented in Figure 1. In fact, some optimizations of the material parameters without the specified boundaries for the Poisson ratios have resulted in a negative value of v_{LR}. This section examines the possibility of having a negative value of v_{LR} on the reference plate where this negative coefficient has been observed which corresponds to longitudinal symmetry configuration 0.

Remembering that the Poisson ratio v_{LR} is defined as the negative ratio of the radial strain to the longitudinal strain as:

$$v_{LR} = -\frac{\varepsilon_R}{\varepsilon_L}$$

The sign of the Poisson ratio can be verified through a tensile test of the reference plate. In particular, A fixed boundary condition is imposed on one of the radial sides of the plate while a distributed force parallel to the longitudinal axis is applied on the opposite side as showed in Figure 3.25.

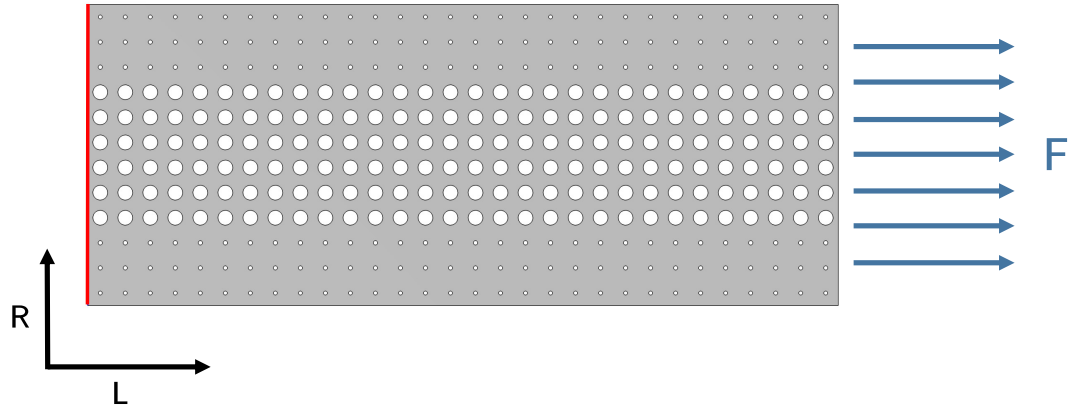

Figure 3.25: Tensile test of the reference plate of configuration 0 with longitudinal symmetry. The side highlighted in red is fixed while a force is applied on the opposite side.

The measured displacements on both the top and bottom longitudinal sides of the plate are displayed on Figure 3.26 below:

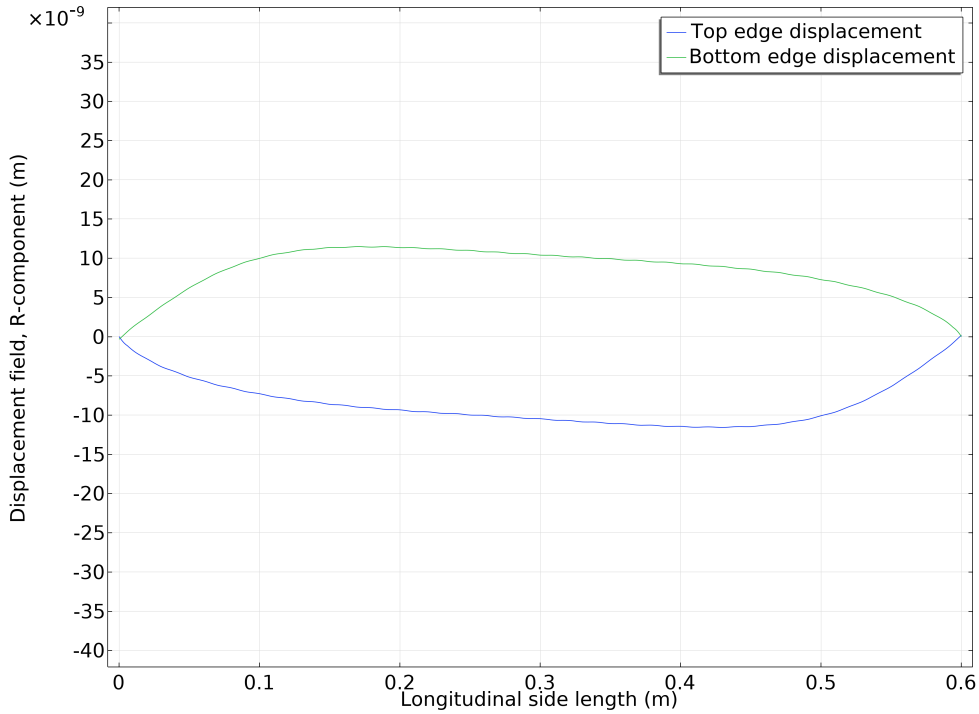

Figure 3.26: Displacement of the top and bottom longitudinal edges as a result of the tensile test.

The figure shows that the bottom side of the plate has a positive displacement while

the top side has a negative one. This means that an elongation of the plate in the longitudinal direction caused a shortening in the radial direction which indicates that the Poisson ratio v_{LR} is indeed positive for this plate. Because this is the only case where a negative Poisson ratio was observed after optimization, the experiment was not repeated for all other configurations and the Poisson ratios were bounded between 0 and 1 for all optimizations.

3.4. Discussing the material parameters of the plates

Having obtained an accurate equivalent plate for all metamaterial configurations considered in this thesis, the aim of this section is to observe the effect of the various studied hole patterns on the material parameters of the wooden plates. Particular attention is given to the values of E_L and E_R as they are the most relevant parameters in terms of impact on the acoustic quality for guitar soundboards [21]. In fact, they can be used to calculate the anisotropy ratio:

$$\frac{E_R}{E_L}$$

as well as the acoustic radiation index defined in [47] and simplified in [21] as:

$$\frac{c_L}{\rho} = \sqrt{\frac{E_L}{\rho^3}}$$

where c_L is the longitudinal sound velocity. In particular, studies have found a correlation between the acoustic quality of woods for soundboards and their anisotropy ratio and acoustic radiation [48]. In addition, the variations of the shear modulus G_{LR} are measured as well due to its impact in the Caldersmith formulas for tuning the frequency of the twisting mode (1,1).

Figures 3.27 and 3.28 illustrate the variations of these three parameters for all configurations k with both longitudinal and radial symmetry. More specifically, they show their normalized value with respect to that of Engelman spruce, the wood species used for the reference plates. In the first figure, the parameters obtained from the application of the Caldersmith formulas are used while the second utilizes the optimized material parameters from the linear density equivalent model.

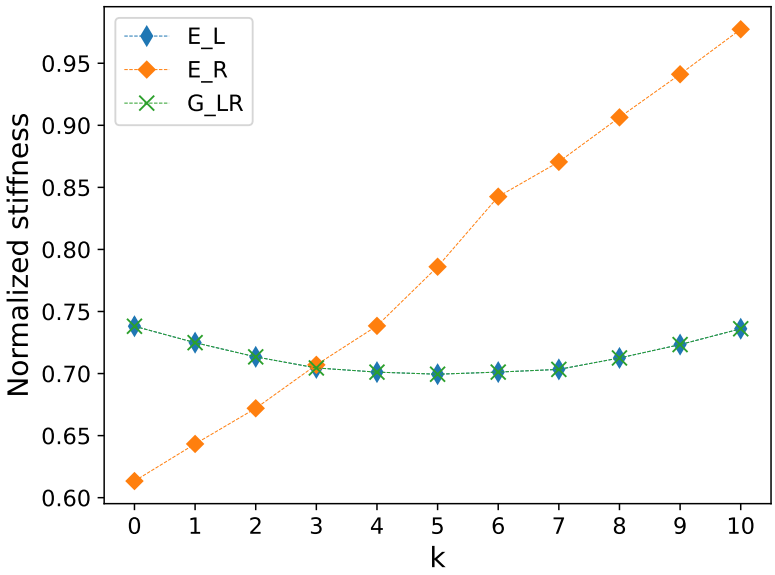

(a) Longitudinal configurations.

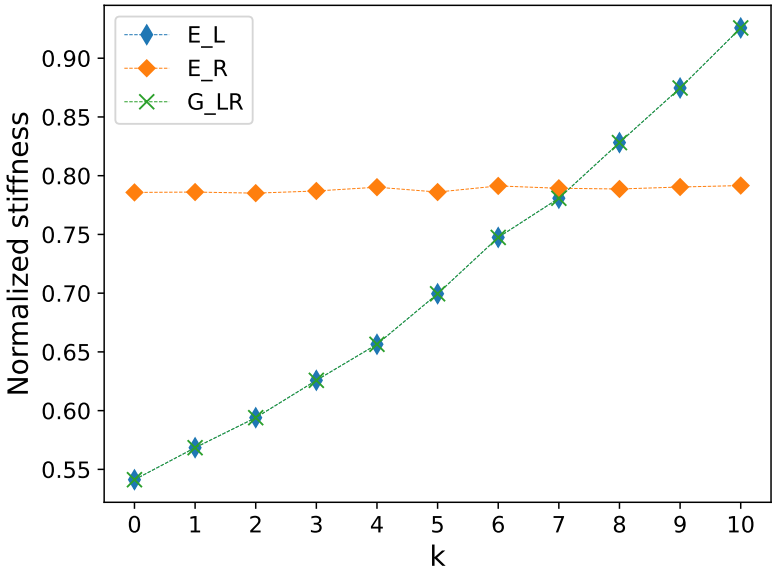

(b) Radial configurations.

Figure 3.27: Normalized value of E_L, E_R, and G_{LR} to the respective stiffness of Engelman spruce for each heterogeneous configuration k obtained using Caldersmith formulas. The values E_L and G_{LR} are superimposed because G_{LR} is calculated using the Wood Handbook formula from Table 2.1 which is proportional to E_L.

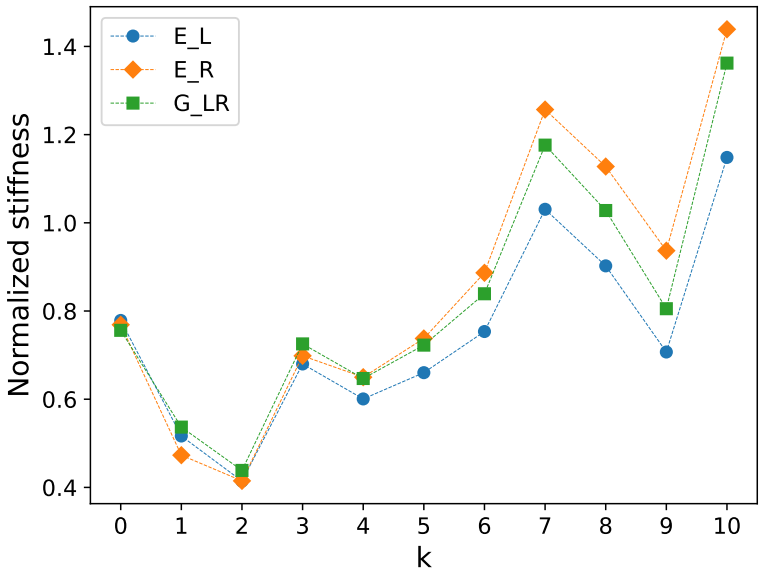

(a) Longitudinal configurations.

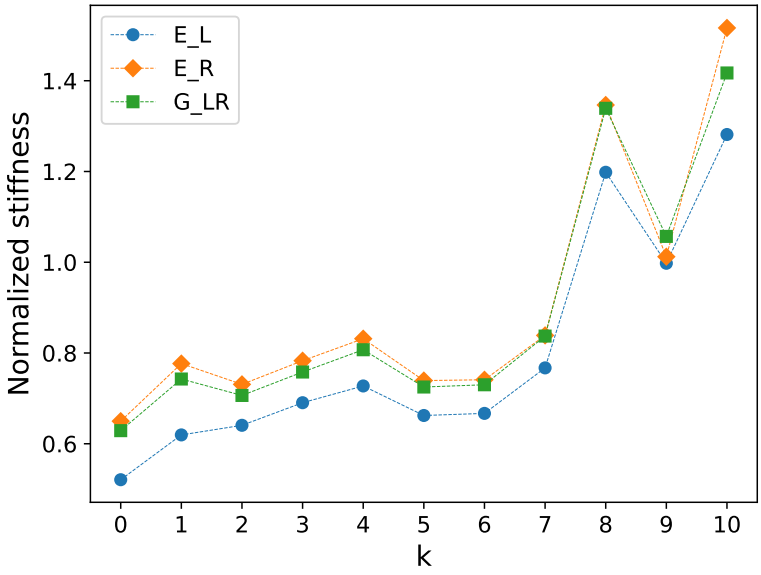

(b) Radial configurations.

Figure 3.28: Normalized value of E_L, E_R, and G_{LR} to the respective stiffness of Engelman spruce for each heterogeneous configuration k obtained from the linear density optimized equivalent plate model.

Upon comparison of the two figures, it is evident that the approximation provided by the Caldersmith method cannot be extended to wooden plates with heterogeneous meta-material patterns. In fact, while similar values of the material parameters are obtained around homogeneous configuration 5 for both the Caldersmtih, and the optimized material parameters, their behaviour for more heterogeneous configurations are completely different.

The most interesting observation to be made from Figure 3.28 is that the general stiffness of the plates seems to be lower for configurations with a lower index k while it is higher as k gets closer to 10 for both longitudinal and radial symmetry configurations. Meaning that plates are made stiffer by patterns with larger hole sizes near the edges and smaller holes at the center of the plate. Probably because having a higher density at the center of the plate increases its stiffness. In some cases, the predicted stiffness is even higher than that of Engelman spruce. Another particular observation on this figure is that the variation between a configuration and the next is similar for the three considered material parameters.

These results highlight the possibility of using the equivalent plates method illustrated in this thesis to control the stiffness and density of a wooden plate. In fact, one of the possible applications could be the design of specifically tuned soundboards by luthiers, giving them the possibility control the general stiffness and density of the board, all while tuning the most important mode shapes to the desired frequencies. This is particularly useful considering that one of the main requisites for achieving a good acoustic radiation with wooden a soundboard consists in having a high stiffness with a lower mass. Not only that, but being able to modulate the stiffness of a wooden board could be used as well in structural applications.

4 | Conclusions and future developments

The objective of this thesis work was to investigate the effects of metamaterials with heterogeneous hole size patterns on the dynamic and static behaviour of rectangular wooden plates. Towards this end, an innovative approach has been used focusing on the study of equivalent solid plates rather than on the actual metamaterial drilled plates. This idea, motivated by the better understanding both engineers and instrument makers have of regular wooden boards which are employed in many musical and structural applications, makes it possible to study the metamaterial's properties under a more familiar perspective. In fact, while other studies in the literature rely on the Caldersmith formulas to approximate the main elastic constants of the metamaterial [21, 22], the method developed here allows for a more precise identification its effective material parameters.

Throughout the thesis, multiple models of equivalent plates have been designed in order to accurately recreate the vibrational behavior of the various heterogeneous metamaterial configurations. More specifically, a finite element model updating optimization method has been implemented in Python to find the material parameters of the equivalent plate which would minimize the difference between the eigenfrequencies and mode shapes of the considered reference and equivalent plates.

The obtained results reveal a striking difference between homogeneous and heterogeneous configurations of the metamaterial. In fact, in the case of a plate with homogeneous hole sizes, and considering the first 37 modes which cover the range up to 1000 Hz, a decent approximation of the elastic constants of the equivalent plate can be obtained by simply applying the Caldersmith formulas with a mean error in the eigenfrequencies of 2.9 %. Using the optimization of the equivalent model with constant density, this error was reduced to 0.3 % with great consistency in the mode shapes as well.

In the case of heterogeneous configurations however, the conducted simulations show that simply varying the elastic constants of the equivalent plate is not sufficient to recreate the metamaterial's behaviour. In fact, the Caldersmith formulas and the constant density

equivalent model deliver poor results regarding the accuracy of the eigenfrequencies and mode shapes. Particularly so for the most heterogeneous configurations. With a varying distribution of the hole sizes on the plate, a corresponding variation in the mass of the equivalent plate must be considered.

Following these results, additional simulations made with a varying thickness equivalent model suggest that modifying the geometry of the plate has too much of an impact on the mode shapes and eigenfrequencies of the plate making it unusable for the purpose of this study. Considering instead a varying density to reflect the mass distribution of the metamaterial seems to yield better results. Of the two considered varying density models, the one with piece wise constant density was shown to increase the complexity of the problem without improving its results while the linearly varying density model proved to be the most efficient one in terms of recreation of the mode shapes and eigenfrequencies of the reference. With a mean error for the first 37 eigenfrequencies of 1.43 % computed over all 22 heterogeneous configurations.

Additionally, a static analysis conducted on both the reference and equivalent plates has shed light on an interesting effect in the studied metamaterial wooden boards. In fact, while the equivalent plates accurately recreate the vibrational behaviour of the corresponding reference configuration, their static behaviour can be different as observed from the carried out stationary tests on the plates. A larger maximum displacement of the board has been observed for the equivalent plates of the most heterogeneous configurations with respect to their reference plate. This different behaviour of the metamaterials' equivalent plates in dynamic and static conditions is an interesting fact which could be used to create custom built instruments in the future.

Finally, this work is concluded with an analysis of the elastic constants of the equivalent plates for all the studied metamaterial configurations. An interesting correlation was found between the stiffness of the wooden board and the hole size distributions on the metamaterial. In fact, having larger holes on the sides of the plate and smaller ones at the center of it resulted in stiffer plates for both longitudinally and radially symmetric configurations. In the most heterogeneous cases, the obtained stiffness was found to be higher than that of Engelman spruce. These result could be of great relevance among other things in the construction of wooden soundboards where a high stiffness is desired to sustain the tension of the strings all while having a low density to maximize sound radiation. In addition, the possibility to tune the eigenfrequencies of the plate using metamaterials which has been demonstrated also in [21, 22] make them a very powerful tool to expand the possibilities of instrument makers. Furthermore, the ability to control the mechanical parameters of any wooden board broadens the range of usable species of

wood in instrument making, offering a sustainable alternative to the most exploited ones in the industry.

The studies exposed in this thesis lend themselves to multiple possible future developments. First of all, an experimental physical study could verify the numerical results and possibly expand on them. As a matter of fact, only elliptical and circular hole shapes have been investigated here. While various orientations and aspect ratios have been studied for the elliptical hole shapes in [21], many other possibilities remain unexplored. It would be interesting as well to see an application of heterogeneous metamaterials in a complete instrument as was done in [36] where homogeneous metamaterials were numerically studied in the model of a classical guitar or in [49] where they were used in a cajòn peruano.

With the recent exponential rise in popularity of artificial intelligence, it is impossible not to think of a possible application in this field of study as well. A potential idea could be the development of an artificial intelligence capable of generating a specific metamaterial configuration of holes in order to tune the mechanical parameters or eigenfrequencies of an initial wooden board. To this aim, the method used in this thesis to obtain accurate solid equivalent plates can be useful for the generation of a large enough numerical data set. Using solid equivalent plates rather than multiple 3D models of different metamaterial configurations could simplify and accelerate the meshing process of the FEM simulations. Such a tool could be easily integrated in the workshop of an instrument maker in the future.

Bibliography

[1] S. Yoshikawa and C. Waltham, "Woods for wooden musical instruments," in *Proceeding of ISMA*, pp. 281–286, 2014.

[2] S. Calvano, F. Negro, F. Ruffinatto, D. Zanuttini-Frank, and R. Zanuttini, "Use and sustainability of wood in acoustic guitars: An overview based on the global market," *Heliyon*, 2023.

[3] A. Pfriem, "Thermally modified wood for use in musical instruments," *Drvna industrija*, vol. 66, no. 3, pp. 251–253, 2015.

[4] J. Lenoir, J.-C. Gégout, P. A. Marquet, P. de Ruffray, and H. Brisse, "A significant upward shift in plant species optimum elevation during the 20th century," *science*, vol. 320, no. 5884, pp. 1768–1771, 2008.

[5] U. G. Wegst, "Wood for sound," *American Journal of Botany*, vol. 93, no. 10, pp. 1439–1448, 2006.

[6] N. Fletcher, "Materials and musical instruments.," *Acoustics Australia*, vol. 40, no. 2, 2012.

[7] F. Dinulică, M. D. Stanciu, and A. Savin, "Correlation between anatomical grading and acoustic–elastic properties of resonant spruce wood used for musical instruments," *Forests*, vol. 12, no. 8, p. 1122, 2021.

[8] T. Ono and M. Norimoto, "On physical criteria for the selection of wood for soundboards of musical instruments," *Rheologica acta*, vol. 23, pp. 652–656, 1984.

[9] M. Quintavalla, F. Gabrielli, and C. Canevari, "Grading materials for stringed instruments soundboards: An approach considering the orthotropic elastic and damping properties," *Applied Acoustics*, vol. 187, p. 108521, 2022.

[10] A. Damodaran, L. Lessard, and A. Suresh Babu, "An overview of fibre-reinforced composites for musical instrument soundboards," *Acoustics Australia*, vol. 43, pp. 117–122, 2015.

[11] M. Mehdi Jalili, S. Yahya Mousavi, and A. S. Pirayeshfar, "Investigating the acoustical properties of carbon fiber-, glass fiber-, and hemp fiber-reinforced polyester composites," *Polymer Composites*, vol. 35, no. 11, pp. 2103–2111, 2014.

[12] C. Besnainou and S. Vaiedelich, "Bow musical instrument made of composite material," Dec. 15 1992. US Patent 5,171,926.

[13] S. A. Ahmed and S. Adamopoulos, "Acoustic properties of modified wood under different humid conditions and their relevance for musical instruments," *Applied Acoustics*, vol. 140, pp. 92–99, 2018.

[14] H. Yano, Y. Furuta, and H. Nakagawa, "Materials for guitar back plates made from sustainable forest resources," *The Journal of the Acoustical Society of America*, vol. 101, no. 2, pp. 1112–1119, 1997.

[15] E. Barchiesi, M. Spagnuolo, and L. Placidi, "Mechanical metamaterials: a state of the art," *Mathematics and Mechanics of Solids*, vol. 24, no. 1, pp. 212–234, 2019.

[16] K. Bertoldi, V. Vitelli, J. Christensen, and M. Van Hecke, "Flexible mechanical metamaterials," *Nature Reviews Materials*, vol. 2, no. 11, pp. 1–11, 2017.

[17] M. R. Haberman and M. D. Guild, "Acoustic metamaterials," *Phys. Today*, vol. 69, no. 6, pp. 42–48, 2016.

[18] S. A. Cummer, J. Christensen, and A. Alù, "Controlling sound with acoustic metamaterials," *Nature Reviews Materials*, vol. 1, no. 3, pp. 1–13, 2016.

[19] C. E. Oñate, A. Arancibia, G. Cartes, and C. F. Beas, "Seeking for spectral manipulation of the sound of musical instruments using metamaterials," in *Proceedings of the 15th International Audio Mostly Conference*, pp. 277–280, 2020.

[20] R. Bader, J. Fischer, M. Münster, and P. Kontopidis, "Metamaterials in musical acoustics: A modified frame drum," *The Journal of the Acoustical Society of America*, vol. 145, no. 5, pp. 3086–3094, 2019.

[21] S. Gonzalez, E. Chacra, C. Carreño, and C. Espinoza, "Wooden mechanical metamaterials: Towards tunable wood plates," *Materials and Design*, vol. 221, p. 110952, 2022.

[22] C. Espinoz, C. Carreño, E. Chacra, and S. Gonzalez, "Metawood: manipulation of the elastic properties of wood plates by periodic hole patterns," in *2022 Sixteenth International Congress on Artificial Materials for Novel Wave Phenomena (Metamaterials)*, pp. 139–141, IEEE, 2022.

[23] M. Lercari, S. Gonzalez, C. Espinoza, G. Longo, F. Antonacci, and A. Sarti, "Using mechanical metamaterials in guitar top plates: a numerical study," *Applied Sciences*, vol. 12, no. 17, p. 8619, 2022.

[24] G. Caldersmith and E. Freeman, "Wood properties from sample plate measurements i," *J Catgut Acoust Soc*, vol. 1, no. series II, pp. 8–12, 1990.

[25] A. F. Bower, *Applied mechanics of solids*. CRC press, 2009.

[26] R. J. Ross, *Wood handbook: wood as an engineering material*. Forest Products Laboratory, 2021.

[27] J. Gómez-Royuela, A. Majano-Majano, A. Lara-Bocanegra, J. Xavier, and M. de Moura, "Evaluation of r-curves and cohesive law in mode i of european beech," *Theoretical and Applied Fracture Mechanics*, vol. 118, p. 103220, 2022.

[28] Z.-F. Fu and J. He, *Modal analysis*. Elsevier, 2001.

[29] I. Firth, "The nature of the tap tone in stringed instruments," *Acta Acustica united with Acustica*, vol. 36, no. 1, pp. 36–41, 1976.

[30] E. F. F. Chladni, *Traité d'acoustique*. Chez Courcier, 1809.

[31] T. Gore, "Contemporary acoustic guitar design and build."

[32] M. McIntyre and J. Woodhouse, "On measuring the elastic and damping constants of orthotropic sheet materials," *Acta Metallurgica*, vol. 36, no. 6, pp. 1397–1416, 1988.

[33] J. N. Reddy, *Introduction to the finite element method*. McGraw-Hill Education, 2019.

[34] S. S. Rao, *The finite element method in engineering*. Butterworth-heinemann, 2017.

[35] G. Longo, "Influence of thickness profile in archtop guitars," Master's thesis, Politecnico di Milano, 2022.

[36] M. Lercari, "A numerical study on mechanical metamaterials in classical guitars," Master's thesis, Politecnico di Milano, 2022.

[37] L. Lodetti, "Parametric modeling and analysis of cello bridges with finite element methods," Master's thesis, Politecnico di Milano, 2023.

[38] COMSOL, "The finite element method (fem)," March 15, 2016.

[39] D. Salvi, "Modal analysis and optimization of the top plate of string instruments

through a parametric control of their shape.," Master's thesis, Politecnico di Milano, 2020.

[40] J. Hennig, M. Elfner, A. Maeder, and J. Feder, "Pythonic scripting interface for comsol multiphysics."

[41] S. Ereiz, I. Duvnjak, and J. F. Jiménez-Alonso, "Review of finite element model updating methods for structural applications," in *Structures*, vol. 41, pp. 684–723, Elsevier, 2022.

[42] M. Pastor, M. Binda, and T. Harčarik, "Modal assurance criterion," *Procedia Engineering*, vol. 48, pp. 543–548, 2012.

[43] R. J. Allemang, "The modal assurance criterion–twenty years of use and abuse," *Sound and vibration*, vol. 37, no. 8, pp. 14–23, 2003.

[44] J. A. Nelder and R. Mead, "A simplex method for function minimization," *The computer journal*, vol. 7, no. 4, pp. 308–313, 1965.

[45] M. J. Powell, "An efficient method for finding the minimum of a function of several variables without calculating derivatives," *The computer journal*, vol. 7, no. 2, pp. 155–162, 1964.

[46] J. E. Mottershead, M. Link, and M. I. Friswell, "The sensitivity method in finite element model updating: A tutorial," *Mechanical systems and signal processing*, vol. 25, no. 7, pp. 2275–2296, 2011.

[47] J. C. Schelleng, "The violin as a circuit," *The Journal of the Acoustical Society of America*, vol. 35, no. 3, pp. 326–338, 1963.

[48] T. Ono, "Frequency responses of wood for musical instruments in relation to the vibrational properties," *Journal of the Acoustical Society of Japan (E)*, vol. 17, no. 4, pp. 183–193, 1996.

[49] G. Marelli, "Metamaterials in instruments making: cajon peruano case study," Master's thesis, Politecnico di Milano, 2022.

List of Figures

List of Tables

List of Symbols

Variable	Description	SI unit
σ_{ij}	stress tensor	Pa
ε_{ij}	strain tensor	-
C_{ijkl}	elastic stiffness tensor	Pa
S_{ijkl}	elastic compliance tensor	1/Pa
E_i	Young's modulus	Pa
G_{ij}	Shear modulus	Pa
v_{ij}	Poisson ration	-
$\boldsymbol{L}$	Longitudinal direction	-
$\boldsymbol{R}$	Radial direction	-
$\boldsymbol{T}$	Tangential direction	-
a	length of the plate	m
b	width of the plate	m
h	thickness of the plate	m
ρ	density of the plate	kg/m^3
$f_{(i,j)}$	frequency of the mode (i,j)	Hz
l	length of the square cells	m
V_h	volume fraction of the hole with respect to the cell	-
k	heterogeneous plates index	-
R	hole radius	m
d	linear density slope	-
x	position in the radial direction	m
L	objective function	-
α	MAC's weight in the objective function	-
i	maximum number frequencies in the optimization	-

Acknowledgements

I would like to thank supervisor Professor Fabio Antonacci for sharing his passion for musical acoustics and and letting me be a part of the laboratory life. It was inspiring to discuss my work with all of its members and see also what other colleagues have been working on. Thank you also for your precious advice and guidance throughout this project.

Particular thanks go as well to my co-advisor Sebastian Gonzalez who has been a solid point of reference during this thesis. Thank you for being present at any time and for passing down your rigorous approach to research.

I would also like to express my thanks to all members of the Cremona acoustics lab who provided me with essential insight concerning my progress, to Emir Chacra for his help on the automatized creation of the reference 3D models, to Carolina Espinoza for her helpful comments on my thesis, to Alexander Brauchler for taking the time to share his results with me, and to Laura Lodetti, a colleague and friend for her constant support. It is always a pleasure to work with you.

To my family, I can never thank you enough for allowing me to study what I love. Even though you were in another country, you were always present, always supportive, and simply the best I could ask for. I love you.

My deepest appreciation goes also to my closest friends for all the laughs, and to all the beautiful souls I met through Polifonia. Music is a great companion, but it only has meaning if shared with others. You are my happiest memory from university.

Finally, I want to say thank you to my neighbour, friend, and polpetta, Alessia. Your silly jokes and endless support are what kept me sane in my most stressful moments. Thank you for bringing just the right amount of crazy to my life. I love you.

As always, praise the sun.